Forest canopy structure and reflectance in humid tropical Borneo: a physically-based interpretation using spectral invariants

Hadi [1,*], Marion Pfeifer [2], Lauri Korhonen [3], Charlotte Wheeler [4], Miina Rautiainen [1,5]

[1] Aalto University, School of Engineering, Department of Built Environment, P.O. Box 14100, 00076 Aalto, Finland

[2] School of Biology, Newcastle University, Ridley Building 2, Newcastle Upon Tyne, NE1 7RU, UK

[3] University of Eastern Finland, School of Forest Sciences, P.O. Box 111, FI-80101 Joensuu, Finland

[4] Department of Geography, University College London, London WC1E 6BT, UK

[5] Aalto University, School of Electrical Engineering, Department of Electronics and Nanoengineering, P.O. Box 15500, 00076 Aalto, Finland

*Corresponding author. Email: hadi.hadi@aalto.fi, tel. +358449362350

Abstract

South East Asia region is a triple hotspot of carbon, biodiversity, and forest degradation. The latter is leading to heterogeneous forest landscapes with predominant and varying intensity of human modification. Optical Earth observation data offers the most feasible and accessible means of mapping and monitoring the forest cover heterogeneity in this region. Further, difficulties in ground data collection in this region present the need for more robust physically-based interpretation of satellite data which extends beyond simple empirical correlations of reflectance data with forest characteristics. We present an application of forest reflectance parameterization based on spectral invariants in lowland humid tropical forests of Malaysian Borneo. Our framework combined field measurements (hemispherical photos) of canopy structure, radiative transfer modelling at leaf (PROSPECT) and canopy scale (PARAS), and assessments using satellite data (Landsat-7 Enhanced Thematic Mapper Plus, ETM+). Field data were collected representing a gradient of forest degradation within a large-scale experimental landscape. Results showed limited ability of Landsat-class satellites to uncover the full gradient of forest degradation in this biome due to similarity in canopy structure as characterized by effective canopy cover, leaf area index, and angular profile of canopy gap fraction. Our findings, however, showed strong expression of leaf optical properties at canopy level. This supports the feasibility to remotely measure canopy biochemistry in dense humid tropical rainforests at medium spatial resolution using freely available Landsat-class satellites, and forthcoming hyperspectral satellite missions.

Keywords: rainforest, South East Asia, degradation gradient, reflectance model, Landsat, canopy cover, leaf area index

1. Introduction

Central to the prescribed solutions in the 2015 historical Paris Climate Agreement (United Nations Framework Convention on Climate Change, 2015) are activities relating to reducing emissions from deforestation and forest degradation (REDD+), the second largest source of global CO_2 emission after burning of fossil fuels (Van der Werf et al., 2009). Tropical regions are well known deforestation hotspots (Hansen et al., 2013; Rudel et al., 2009). It has been estimated that tropical forest conservation and restoration could provide half of the target net emission reduction (Houghton et al., 2015). In particular, the humid tropical rainforests of insular South East Asia region, which are among the world's most carbon-rich forests (Avitabile et al., 2016; Sullivan et al., 2017), are also historically and presently under the largest threat of deforestation and forest degradation (Gaveau et al., 2016; Koh et al., 2011; Margono et al., 2014). This region's forests have been shown to have higher aboveground biomass (Slik et al., 2010) and deforestation rate (Margono et al., 2014) than the Amazonian.

Most developing countries, which are home to the majority of the world's tropical forests, lack the financial capacity to undertake regular ground-based national forest inventory and monitoring. Remote sensing using the suite of operational passive optical Earth observation (EO) satellites is presently the most viable technology to map and monitor (also in near-real-time) tropical forests structure in operational manner (DeVries et al., 2015; MacDicken, 2015; Popkin, 2016). As an example, in Brazilian Amazon several operational forest monitoring systems based on Landsat and MODIS (Moderate Resolution Imaging Spectroradiometer) satellites are in place (Wheeler et al., 2014). Furthermore, the recent launch of new generation optical satellite Sentinel 2 (A and B), with unprecedented spatial (10 meters in visible bands) and temporal (5 day revisit time at the equator) resolution among its class, would potentially provide improved tropical forests mapping and monitoring capabilities in the near future.

Additionally, synergic use of both Sentinel 2 and Landsat is currently under development (see https://hls.gsfc.nasa.gov/) and when ready, will further increase the temporal resolution and consequently improve cloud-free data availability in tropical regions. Other types of remote sensing such as active radar and lidar are also actively developed, but their operational use for large area mapping and monitoring in tropical regions is not foreseeable in the near future. In addition to data availability, processing and interpretation (e.g., visual) of radar and lidar data can be technically more demanding, and thus not as accessible as optical data to local management staff in the tropics.

Optical EO data has been used in South East Asian rainforests primarily to map deforestation (Hansen et al., 2013; Margono et al., 2014) and to discriminate basic forest classes i.e., primary (intact) and disturbed (logged) forests (Wijedasa et al., 2012) or, with visual interpretation, forest and oil palm (Carlson et al., 2012; Gaveau et al., 2016). Beyond classification-based analysis, optical EO data has been used, to a smaller extent, in the estimation of forest above ground biomass (Basuki et al., 2012; Langner et al., 2012; Pfeifer et al., 2016; Propastin, 2013), fractional vegetation cover and leaf area index (Pfeifer et al., 2016; Propastin and Erasmi, 2010). The latter type of analysis estimating forest structure as a continuous variable is particularly important to uncover the spatial heterogeneity of modern forest landscape in insular South East Asia, the result of widespread forest degradation (i.e. the second "D" in REDD+).

Man-made degradation processes such as selective logging at different intensities alter canopy structure through partial sub-canopy removal of tree cover. Canopy structure refers to the amount and organization of phytoelement in the canopy (Welles and Cohen, 1996). The amount is typically characterized with canopy cover or leaf area index. A recent study in Sabah, Borneo using airborne lidar data showed canopy cover, or its complementary canopy gap fraction, to

be closely related to basal area, which improved aboveground carbon density estimation (Coomes et al., 2017). The phytolement organization is mainly observed as the different degrees of foliage clumping in the canopy. The clumping in turn influences canopy gap fraction in different directions as trees organize their branches and leaves to capture lights, while co-occupying the canopy space with other trees. Information on canopy structure (amount and organization) is essential on one hand to characterize the light (radiation) regime within the forest (Ross, 1981) as well as forest microclimate (Hardwick et al., 2015), and on the other hand for interpretation of remotely sensed forest reflectance (Nilson, 1999). Directional gap fraction determines how much light gets intercepted by the canopy, how much gets transmitted to forest floor, and how much is scattered escaping the canopy towards the sensor. Further, the angular profile of gap fraction allows to quantify the daily integration of light interception as sun zenith angle changes. To our knowledge, the gap fraction profiles of South East Asia rainforest canopy, especially the human-modified forest areas, have not been reported in previous studies.

Estimation of forest structural variables in humid tropical South East Asia using optical satellite data has been primarily done by empirical statistical modelling with spectral vegetation indices, and semi-empirical spectral mixture analysis. Although simple to implement, empirical methods are at best locally accurate i.e., they are site and sensor specific. In other words, empirical predictive models cannot be easily transferred to other forest areas, especially in the highly heterogeneous tropical forest environment (Foody et al., 2003). More robust physically-based remote sensing interpretation methods are needed for large scale extrapolation mapping, especially for complex tropical forests where sizable field data collection is challenging. Equally importantly, physically-based models also provide mechanistic understanding of factors driving forest reflectance (Verstraete et al., 1996), another missing knowledge concerning South East Asian tropical forest. Unsurprisingly, physically-based models are the

preferred retrieval approach in operational satellite-based global vegetation parameters products, such as the MODIS LAI/FPAR (Myneni et al., 2002) and SPOT-VEGETATION GEOV1 LAI/FAPAR/FCOVER (Baret et al., 2013). However, physically-based approaches are very rarely applied in tropical forest (see e.g., application review of the widely-used PROSAIL model in Jacquemoud et al., 2009).

A small number of attempts on physically-based forest reflectance modelling have been carried out within tropical forest context. Asner and Martin (2008) applied canopy reflectance model designed for high resolution (< 3 m) airborne hyperspectral imaging data to upscale measured leaf optical properties to canopy level in Australian rainforests, using canopy structural variations which are typical in humid tropical forests as identified from literature sources. Their aim was to investigate the impact of the prescribed canopy structural properties on leaf constituents (e.g., pigments) retrieval from canopy spectra. In another study Féret and Asner (2011a) upscaled leaf optical properties (simulated using measured leaf chemicals and a leaf radiative transfer model) to canopy level (using literature values of canopy structural variations) in humid forests of Hawaii to investigate species classification from canopy spectra. To our knowledge, application of physically-based forest reflectance models at the spatial and spectral resolution of currently operational Landsat-class sensors has not been demonstrated. Furthermore, the results of reflectance modelling in previous studies were not always validated with satellite data.

The limited application of physically-based forest reflectance models in the tropical region owes to a large extent the many model parameters not all readily measured in the field. For example, the SLC (Soil-Leaf-Canopy) or 4SAIL2 model (Verhoef and Bach, 2007) requires as input, among others, the leaf angle distribution parameters and tree shape factor which are likely

151 species specific and thus difficult to parameterize in tropical forest with high species diversity.
152 Complex reflectance models require a large set of independent free parameters (state variables),
153 which in turn require prior expert guesses or ancillary information of their values. Due to this,
154 complex reflectance models are more likely to not have a unique and ecologically meaningful
155 inversion solution (i.e., different combination of inputs producing similar forest reflectance),
156 and are much more computationally expensive (Verstraete et al., 1996). To this end, the
157 recently introduced forest bidirectional reflectance factor (BRF) parameterization based on the
158 novel spectral invariants theory (Stenberg et al., 2016) called the PARAS model (Rautiainen
159 and Stenberg, 2005) is particularly advantageous within tropical forest context owing to its
160 alternative simple parameterization requiring minimum expert guesses for the inputs. An
161 additional advantage of PARAS forest reflectance parameterization lies in its ability to
162 explicitly and intuitively decouple the contribution to canopy-level BRF from phytoelement
163 (e.g., leaf) optical properties, and from canopy structure (Knyazikhin et al., 2013; Latorre-
164 Carmona et al., 2014) at different scales of phytoelement organizations (Schull et al., 2011).
165 The leaf-level contribution i.e. the extent that leaf optical properties are expressed at the
166 remotely sensed canopy scale is especially of interest within the context of tropical forests as
167 they serve as a proxy to leaf biochemistry (Asner and Martin, 2016). To date the use of spectral
168 invariants in modelling canopy BRF has been demonstrated in a wide range of forest in
169 temperate and boreal region (Stenberg et al., 2016). The method is operationally used in the
170 MODIS global leaf area index (LAI) algorithm (Myneni et al., 2002) and for the ongoing
171 development of a Landsat-based global LAI product (Ganguly et al., 2012).
172
173 In this study, we present the first application and validation of physically-based forest canopy
174 BRF parameterization based on spectral invariants (PARAS model) in humid tropical forests
175 of insular South East Asia. We used field measurements of canopy structure by the means of

hemispherical photography from a forest fragmentation landscape in Malaysian Borneo, providing a dataset encompassing forests which have experienced varying degrees of degradation, as well as oil palm plantations. We first examined canopy structure of the different forest degradation classes, and their relationship with canopy BRF (surface reflectance) recorded by Landsat-7 Enhanced Thematic Mapper Plus (ETM+). Second, we modelled BRF of the closed-canopy forest plots at the operational Landsat-class spatial (i.e., stand level of 30 × 30 m) and (multi)spectral resolution using PARAS. Third, we subsequently assessed the modelled BRF against satellite BRF via root mean squared difference and analyzed the variability in BRF induced by variability in leaf optical properties. Fourth, we applied a global sensitivity analysis to the PARAS model in order to simultaneously quantify the relative contribution from leaf optical properties and canopy structure to remotely sensed canopy-level BRF.

2. Materials and method

2.1. Field measurements

Field measurements of canopy structure were carried out in the Stability of Altered Forest Ecosystem (SAFE) forest degradation landscape located in Sabah, lowland Malaysian Borneo (Ewers et al., 2011; Figure 1a). The climate at the equatorial SAFE landscape is aseasonal and no dry months were recorded between September 2011 and January 2013 (Pfeifer et al., 2016). The SAFE project area consists of unlogged forest (in the Maliau Basin Conservation Area), logged forest, and oil palm plantation. Field measurement plots were established in sampling blocks (Figure 1b), namely primary old growth forest (blocks OG1 and OG2), lightly logged forests in a virgin jungle reserve and multi-use forest (VJR and OG3), twice logged forests in mount Louisa Forest reserve (LFE, LF1, LF2, and LF3), salvage logged forest (A, B, C, D, E, and F), and oil palm plantation (OP1, OP2, and OP3). Canopy hemispherical photos were

acquired in 172 permanent sampling plots (25 × 25 m, 12–13 photos per plot) following standard protocols as implemented in the Global LAI project (https://globallai.files.wordpress.com/2015/09/pfeifer_2015_protocol_lai_measurements_v3-0.pdf). The combined survey area covered more than two hectares. The plots were located avoiding slopes and preserving distance from forest edges. Canopy photographs were taken between August 2012 and August 2013. The camera system used was Canon EOS 5D Mark II with sigma 8mm f3.5 EX DG circular fisheye lens. The photos were acquired 1 m above ground level, the upper margin facing northward. As large canopy openings were not often available on site, we primarily relied on exposure adjustment in reference to the measured in-stand automatic exposure (Pfeifer et al., 2014, 2012; Zhang et al., 2005). At each sampling point, three photos were taken at three different exposures i.e., 0 (Auto), -1 (Underexposure), and +1 (Overesposure). We then visually selected the photos which gave the best contrast between the canopy and background sky.

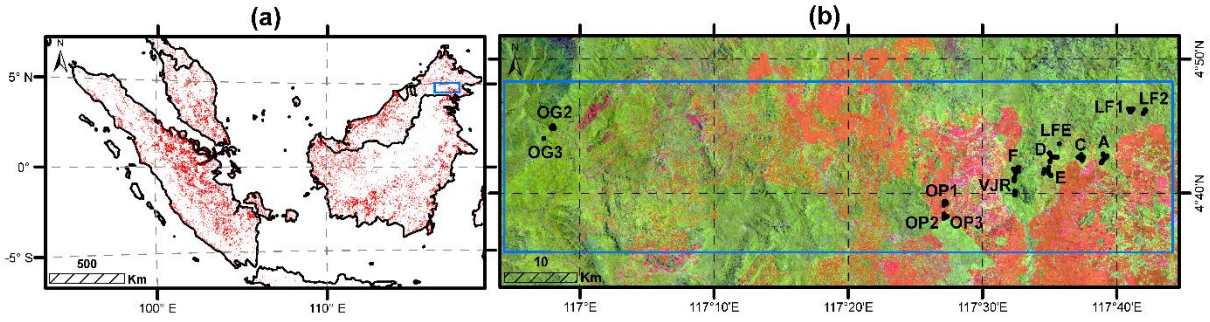

Figure 1. Map of study area. (a) Insular South East Asia showing Borneo island and SAFE project site (blue rectangle, not to scale). Land boundaries are from www.thematicmapping.org provided by Bjorn Sandvik. Areas in red show Landsat-derived forest loss during 2000-2012. (b) Distribution of vegetation plots used in this study. The label shows their respective sampling blocks explained in text. Background image is Landsat 7 cloud-free composite (SWIR1, NIR, red) ca. 2012. The red areas are forest loss as in (a). Forest loss map and Landsat image

composite obtained from Hansen et al. (2013, data source Hansen/UMD/Google/USGS/NASA version 1).

Due to limited availability of cloud- and haze-free satellite observations, as well as gaps in image due to scan line failure of ETM+ sensor used, 88 plots could be used in this study (Figure 1b). Our plots covered both forest and plantation biomes. The forest overstory was dominated by tree species belonging to the *Dipterocarpaceae* family. The plots were classified into six forest classes based on degradation status: primary forest, lightly logged forest, twice logged forest, salvage logged forest stage 1, salvage logged forest stage 2, and oil palm plantation. The forest classes are described in Table 1. Figure A1 in Appendix A shows example hemispherical photos of the different forest classes.

Table 1. Description of forest degradation classes.

Forest classes	No. of plots	Description
Primary	5	Mature and undisturbed forest.
Lightly logged	8	Lightly or illegally logged forests inside multi-use or protected areas.
Twice logged	14	Forest area that has been selectively logged once during 1970s, followed by a second logging round from the late 1990s to the early 2000s.
Salvage logged stage 1	26	Forest area that has been logged with lifted restrictions on type of tree, size limits and volume in advance of outright conversion to a new land use type such as agriculture.
Salvage logged stage 2	23	Salvage logged forests which were being converted to fragmented agricultural landscape ("poor" and "very poor" forest quality, see Ewers et al., 2011).
Oil palm	13	Managed oil palm plantation planted in 2000 (2 plots) and 2006 (11 plots).

2.2. Satellite data

We used the available Landsat-7 Enhanced Thematic Mapper Plus (ETM+) surface reflectance (i.e., bidirectional reflectance factor, BRF) Climate Data Record (US Geological Survey, 2016) obtained from the USGS on-demand processing system EROS Science Processing Architecture (ESPA, https://espa.cr.usgs.gov/). The surface reflectance product is processed from Level 1 radiometric, geometric, and terrain corrected (L1T) top-of-atmosphere reflectance using the Landsat Ecosystem Disturbance Adaptive Processing System (LEDAPS) processing (Masek et al., 2006). The ETM+ sensor records reflected radiance in seven (7) spectral bands namely blue (450 – 520 nm), green (520 – 600 nm), red (630 – 690 nm), near-infrared (NIR, 770 – 900 nm), shortwave-infrared 1 (SWIR1, 1550 – 1750 nm), and shortwave-infrared 2 (SWIR2, 2090 – 2350 nm). These bands have 30 m spatial resolution.

Three image scenes from the same period as field measurements were used (Table 2). After filtering out all pixels not flagged as 'clear' (i.e. cloud, cloud-shadow, water pixels) in the 'cfmask' layer provided with the SR product, we further filtered out hazy pixels using the accompanying atmosphere opacity layer (values > 0.3 are interpreted as hazy observation, Claverie et al., 2015). This ensured only pixels with as minimum atmospheric noise residual as possible were used, considering forest fire is a recurring event in the surrounding region. BRFs were then extracted from the pixel corresponding to field plot location using "raster" library (Hijmans, 2016) in R statistical environment (R Core Team, 2016).

Table 2. Satellite data (Landsat-7 ETM+).

Field date of used plots	Image date	Scene ID	Sun zenith angle (°)
Aug 2012 – Dec 2012	27 Aug 2012	LE71170572012240EDC00	28.2
	1 Dec 2012	LE71170572012336EDC00	35.5
	17 Dec 2012	LE71170572012352EDC00	37.8

2.3. Estimation of canopy structural variables from hemispherical photos

The digital hemispherical photos were thresholded (i.e., classified into canopy vs. background sky pixels) using the global clustering method (Ridler and Calvard, 1978) as recommended in Jonckheere et al. (2005). We rigorously checked each classified (binary) image visually, and noticed that six plots had 1-3 photos excluded due to severe misclassification or sunfleck problem. Next we calculated annular canopy gap fraction in five view zenith rings (0 – 15°, 15 – 30°, 30 – 45°, 45 – 60°, and 60 – 75°) pertaining to the LAI-2000 Plant Canopy Analyzer (Li-Cor Inc., Nebraska, USA) instrument. Effective leaf area index, LAI_{eff} (Chen et al., 1991) was calculated from the gap fraction using the method employed by LAI-2000 (Welles and Norman, 1991). We note that the LAI-2000 algorithm may partially account for clumping with the Lang and Xiang (1986) logarithmic gap averaging method, as shown from the extensive database from other vegetation biomes compiled by Ryu et al. (2010). We also calculated effective canopy cover, ECC (Rautiainen et al., 2005) approximated as one minus canopy gap fraction in the near-vertical direction i.e. first ring (0 – 15°), and angular canopy closure over 0 – 75° view zenith angles (rings 1 – 5), ACC_{75} (Korhonen et al., 2011). The photos were processed using a self-written Matlab (MathWorks) routine (Korhonen et al., 2011).

LAI_{eff} assumes random spatial distribution of canopy phytoelements. To correct for natural non-randomness (clumping) of canopy elements i.e., to obtain 'true' leaf area index (LAI_{true}), we calculated canopy clumping index (CI) so that $LAI_{true} = LAI_{eff} / CI$. CI ranges from 0 to 1, the smaller value indicates higher degree of clumping. CI was calculated using the method by Chen and Cihlar (1995) and Leblanc (2002) which utilizes both gap fraction and gap size information . This method is advantageous over the Lang and Xiang (1986) method in that it does not assume spatial distribution pattern of foliage clumps and is therefore suitable for all types of

canopy. In principle, it computed CI by comparing the measured accumulated canopy gap fraction against the gap fraction for a theoretical canopy with the same LAI_{eff} but with randomly distributed foliage elements (i.e., removing large canopy gaps not theoretically possible in a random canopy). We used the freeware CIMES with batch processing (Gonsamo et al., 2011, http://jmnw.free.fr/) to calculate CI. Note that the above estimated LAI strictly speaking refers to total plant area index as it included both foliage and woody (non-photosynthetic) canopy elements. We did not apply a woody area correction as it was not measured. Measurements of woody area index require direct harvest (which was not practically possible in our study sites) and there are no reported values in the literature for the studied forest area and tree family.

2.4. Modelling forest reflectance

In the PARAS model, photon-vegetation interactions within forest canopy medium are modelled using a single spectrally invariant parameter called the photon recollision probability *p* (Smolander and Stenberg, 2005) which is a summary descriptor of canopy structure. Importantly, the *p* parameter can be estimated mainly from canopy gap fraction, which in turn can be relatively quickly measured with digital hemispherical (fisheye) camera or LAI-2000 Plant Canopy Analyzer. The simple analytical formulation of the PARAS model provides another advantage in terms of computational speed, allowing simulations for a large number of scenarios (e.g., forest structure and species). Despite the simplification, in its previous applications PARAS model has been shown to achieve similar or even better accuracy compared to more complex reflectance models, such as DART (Gastellu-Etchegorry, 1996) for estimating spruce leaf chlorophyll content (Yáñez-rausell et al., 2015), and FRT (Kuusk and Nilson, 2000) for estimating coniferous forest total shortwave albedo (Stenberg et al., 2013; Kuusinen et al., 2014).

In the PARAS model (Rautiainen and Stenberg, 2005), the canopy-level BRF is calculated as the sum of BRF originating from the ground, and canopy components:

$$\mathrm{BRF} = \mathrm{cgf}(\theta_{\mathrm{view}})\ \mathrm{cgf}(\theta_{\mathrm{sun}})\ \rho_{\mathrm{ground}} + Q\ i_0(\theta_{\mathrm{sun}})\ \omega_C \quad (1)$$

The first term in Eq. (1) represents the ground contribution to canopy BRF. $\mathrm{cgf}(\theta_{\mathrm{view}})$ and $\mathrm{cgf}(\theta_{\mathrm{sun}})$ are canopy gap fraction (direct, uncollided transmittance) in, respectively, sensor viewing θ_{view} and Sun illumination θ_{sun} zenith angles). The bidirectional gap probability, that is the probability of the sensor viewing sunlit ground, is thus $\mathrm{cgf}(\theta_{\mathrm{view}}) \times \mathrm{cgf}(\theta_{\mathrm{sun}})$. ρ_{ground} is reflectance factor of ground. See Table 3 for complete formulae description.

The second term in Eq. (1) represents the BRF contribution from the canopy. $i_0(\theta_{\mathrm{sun}})$ is canopy direct (zero order) interceptance in Sun direction ($i_0(\theta_{\mathrm{sun}}) = 1 - \mathrm{cgf}(\theta_{\mathrm{sun}})$). ω_C is the canopy scattering coefficient linked to leaf single scattering albedo ω_L through photon recollision probability p. p is defined as the mean probability that a photon scattered by a leaf (phytolement) within the canopy will again interact with another leaf within (instead of escaping) the canopy. Q is the fraction of radiation scattered upwards from the canopy towards the sensor.

Table 3. List of inputs and formulas used to simulate forest BRF with the PARAS model.

Model inputs	Details
Canopy gap fraction in sun illumination direction ($\mathrm{cgf}(\theta_{\mathrm{sun}})$)	θ_{sun} is identified from satellite image metadata i.e., sun zenith angle in Table 2; $\mathrm{cgf}(\theta_{\mathrm{sun}})$ was linearly interpolated based on $\mathrm{cgf}(\theta_{0\text{-}15^\circ})$ and $\mathrm{cgf}(\theta_{15\text{-}30^\circ})$.
Canopy direct (zero order) interceptance ($i_0(\theta_{\mathrm{sun}})$)	$i_0(\theta_{\mathrm{sun}}) = 1 - \mathrm{cgf}(\theta_{\mathrm{sun}})$.

Canopy gap fraction in sensor view direction (cgf(θ_{view}))	Nadir view direction for Landsat i.e. cgf(θ_{view}) = cgf($\theta_{0\text{-}15°}$).
Diffuse non-interceptance (DIFN)	DIFN = 0.066 cgf($\theta_{0\text{-}15°}$) + 0.189 cgf($\theta_{15\text{-}30°}$) + 0.247 cgf($\theta_{30\text{-}45°}$) + 0.249 cgf($\theta_{45\text{-}60°}$) + 0.249 cgf($\theta_{60\text{-}75°}$); based on LAI-2000 method.
Effective leaf area index (LAI_{eff})	Calculated from annular gap fractions estimated from hemispherical photos using the LAI-2000 method.
Canopy clumping index (CI)	Gap size distribution method of Chen and Cihlar (1995). Calculated using CIMES software (Gonsamo et al., 2011), routine LAIMIL.
True leaf area index (LAI_{true})	$LAI_{true} = LAI_{eff} / CI$.
Average photon recollision probability (p)	$p = 1 - \frac{1 - DIFN}{LAI_{true}}$; Stenberg (2007)
Leaf single scattering albedo (ω_L)	Albedo = reflectance + transmittance. Simulated using PROSPECT-4 leaf reflectance and transmittance model (Feret et al., 2008) and published leaf constituents measurements of dominant tree family *Dipterocarpaceae* (Asner et al., 2012).
Fraction of upward scattered radiation (Q)	$Q = \frac{1}{2} + \frac{q}{2}\left(\frac{1 - p\,\omega_L}{1 - p\,q\,\omega_L}\right)$; asymmetry parameter $q = 1 - e^{(-0.1684\ LAI_{true})}$; Mõttus & Stenberg (2008).
Canopy scattering coefficient (ω_C)	$\omega_C = \omega_L \frac{1 - p}{1 - p\,\omega_L}$; Smolander and Stenberg (2005).
Ground reflectance (ρ_{ground})	Obtained from ISRIC world soil information database (plot code ID 15)

For the forest reflectance modelling, canopy structural inputs were obtained from field measurements with digital hemispherical photography, while ground and leaf spectral inputs were obtained from literature (Table 3). Ground reflectance ρ_{ground} was obtained from the available ISRIC (International Soil Reference and Information Center) world soil information database, global VNIR soil spectral library (World Agroforestry Center). Soil reflectance spectra collected in Bukit Raya Nature Reserve primary forest, Central Kalimantan (Indonesian

335 Borneo) was used (Van Reuler, 1987 in Bruijnzeel et al., 1995). The spectra (6 samples) were
336 measured from 350 to 2500 nm at 10 nm interval. The spectra (Figure 2) were resampled to
337 Landsat-7 ETM+ bands using ETM+ sensor response function.

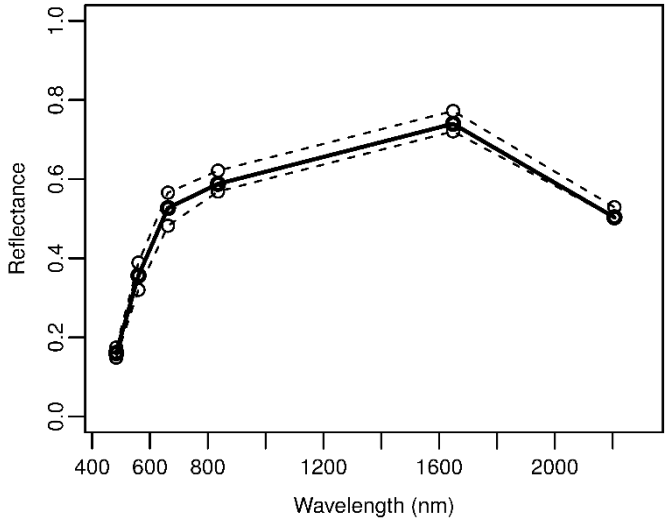

338

339 Figure 2. Measured forest soil reflectance (minimum, mean, maximum) in Borneo.

340

341 Leaf albedo (ω_L) for forest plots was modelled using the leaf reflectance and transmittance
342 model PROSPECT version 4 (Jacquemoud et al., 2009) using as inputs the measured leaf
343 constituents of family *Dipterocarpaceae* collected at Lambir Hills National Park, Sarawak,
344 Borneo (Asner et al., 2012). *Dipterocarpaceace* is the dominant family, and largely accounts
345 for leaf biochemical diversity in the area (Asner et al., 2012). Unfortunately, we could not carry
346 out modelling for oil palm plots due to unavailability of needed leaf optical or biochemical
347 constituents data.

348

349 PROSPECT models leaf directional-hemispherical reflectance ($R_{mod}(\lambda)$) and transmittance
350 ($T_{mod}(\lambda)$) over the optical domain from 400 to 2500 nm at 1 nm interval. PROSPECT-4 requires
351 as input chlorophyll a and b content (C_{ab}), equivalent water thickness (EWT or C_w), dry matter
352 content (C_m, equals leaf mass per area, LMA) and leaf mesophyll structure N:

$$[R_{mod}(\lambda), T_{mod}(\lambda)] = \text{PROSPECT-4}\ (N, C_{ab}, C_m, C_w) \quad (2)$$

We converted the mean leaf constituents reported in Asner et al. (2012) on per mass (concentration) basis, to per area (content) basis required by PROSPECT model: C_{ab} (µg cm^{-2}) = C_{ab} (mg g^{-1}) × C_m (g m^{-2}) × 0.1; C_m (g cm^{-2}) = C_m (g m^{-2}) × 0.0001; C_w (g cm^{-2}) = C_m (g cm^{-2}) × Cw (% fresh mass) × 0.01 × (100 / (100 - C_w)). N was fixed to 1.7 which was the value used for fresh leaves in Jacquemoud et al. (1996). We compared the modelled *Dipterocarpacea* family leaf albedo (= $R_{mod}(\lambda)$ + $T_{mod}(\lambda)$), and leaf albedo modelled with the only publicly available (to our knowledge) tropical leaf constituents data from Hawaii (Feret et al., 2008) to preliminarily verify that the modelled leaf albedo was not unrealistic (Figure 3).

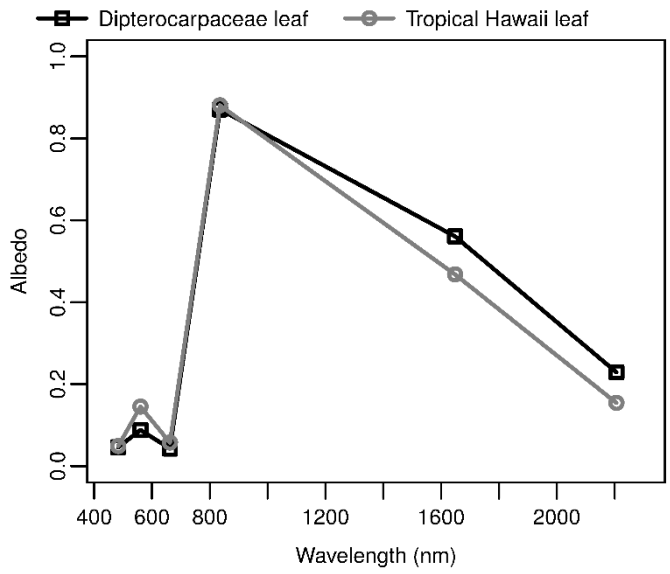

Figure 3. Leaf albedo modelled using PROSPECT-4. The spectra are resampled to Landsat-7 ETM+ bands.

Next, we modelled variability in leaf albedo by varying leaf constituents (i.e., PROSPECT inputs). According to the publicly available ANGERS leaf database (obtained from http://opticleaf.ipgp.fr/index.php?page=database, Feret et al., 2008) the leaf constituents

variability reported on per-mass basis does not equal variability on per-area basis. Therefore, we applied the range of leaf constituents reported on per-area basis, as required by PROSPECT, for the only publicly available leaf dataset of tropical tree species from Hawaii in Feret et al. (2008). In practice, we calculated the Hawaii leaf constituent minimum and maximum values as percentages from the mean, and applied these percentages to the *Dipterocarpaceae* family mean leaf constituent to estimate its minimum and maximum leaf constituents (Table 4). The range (minimum, maximum) relative to mean values were 37.4%, 155.2% for C_{ab}; 46.2%, 259.3% for C_w; and 51.2%, 183.2% for C_m. Based on the minimum and maximum leaf constituents, we generated 2500 samples of leaf constituents combinations from the multivariate uniform distribution of leaf constituents. To exclude unrealistic leaf constituents combinations, we applied the global leaf constituents (per area) correlation published in Feret et al. (2011b).

Table 4. Leaf constituents of *Dipterocarpaceae* family used in PROSPECT-4 to model leaf albedo. C_{ab} is chlorophyll a and b content, C_w equivalent water thickness, C_m dry matter content.

Statistics	C_{ab} (µg cm^{-2})	C_w (g cm^{-2})	C_m (g cm^{-2})
Mean	75.09	0.0152	0.0139
Minimum	28.08	0.0070	0.0071
Maximum	116.54	0.0393	0.0254

PROSPECT modelling was implemented using "Rprospect" library (Serbin, 2013) in R (R Core Team, 2016). Spectral resampling was done using "hsdar" library (Lehnert et al., 2016) in R (R Core Team, 2016). PARAS model was implemented in R (R Core Team, 2016).

2.5. Data analysis and validation of PARAS simulations

First, we tested statistical significance of differences in canopy structure among forest classes. Due to unequal sample sizes (number of plots) among the groups (forest classes) which may cause non-homogeneity of variances in each of the groups (tested using Bartlett's K-squared test), we compared the means of canopy structural variables between forest classes using t-test with Welch correction in R "stats" library (R Core Team, 2016). The Bartlett's test was used to compare variances in canopy structural variables.

Next, we evaluated the performance of PARAS model using satellite data. The satellite-measured (Landsat-7 ETM+) BRF is at best an approximation of true surface reflectance due to possible residual errors such as from atmospheric correction. We assessed the BRF modelled with PARAS model against the BRF measured by Landsat-7 satellite based on root mean square difference (RMSD), mean difference (MD, i.e., bias), and RMSD corrected for bias (RMSDC):

$$\mathrm{RMSD} = \sqrt{\frac{1}{n}\sum_{i=1}^{n}(\mathrm{BRF_{mod}} - \mathrm{BRF_{obs}})^2} \quad (3)$$

$$\mathrm{MD} = \frac{1}{n}\sum_{i=1}^{n}(\mathrm{BRF_{mod}} - \mathrm{BRF_{obs}}) \quad (4)$$

$$\mathrm{RMSDC} = \sqrt{\frac{1}{n}\sum_{i=1}^{n}(\mathrm{BRF_{mod}} - \mathrm{BRF_{obs}} - \mathrm{MD})^2} \quad (5)$$

The overall discrepancy (RMSD) between modelled and observed BRF is therefore decomposed into systematic bias (MD, overall difference in levels of BRF) and random unsystematic discrepancy (RMSDC) i.e., $\mathrm{RMSD} = \sqrt{\mathrm{MD}^2 + \mathrm{RMSDC}^2}$.

2.6. Global sensitivity analysis

We quantified the relative contribution of PARAS model inputs to the modelled canopy-level BRF using global sensitivity analysis (GSA) which simultaneously varies all inputs and accounts for non-linear output-input dependence (Iooss and Lemaître, 2015). We computed the variance-based (sobol) total effect indices (Saltelli et al., 2010; Sobol, 1993) which measure the contribution of each input to the variability in output, accounting for the input's interactions with other inputs (first and higher order effects). The PARAS (first order) inputs considered were LAI_{eff}, canopy direct interceptance $i_0(\theta_{sun})$, gap fraction in sensor view direction $cgf(\theta_{view})$, leaf albedo ω_L, and ground reflectance ρ_{ground}; the first three represent canopy structural attributes which influence canopy BRF. We generated 20000 sobol (quasi-Monte Carlo) sequences (samples) of the investigated model inputs based on the range of inputs' values obtained from measurements (canopy structural attributes derived from hemispherical photos) or literature (soil reflectance, PROSPECT-modelled leaf albedo). GSA was implemented using 'sobolJansen' (Jansen, 1999) routine in the 'sensitivity' package (Pujol et al., 2017) in R statistical environment (R Core Team, 2016).

3. Results

3.1. Canopy structure

Overall, the canopy of primary, lightly logged, and twice logged forest plots were structurally similar, with very little (not significant, $P > 0.01$) difference in all of the canopy structural variables (Table 5). Compared to primary, lightly logged, and twice logged forests, salvage logged forests had lower canopy cover and LAI (significant, $P < 0.01$). Intensively salvage logged forests ("Stage 2") also had more clumped canopies, as indicated by lower CI values (significant, $P < 0.01$). Salvage logged stage 2 plots also displayed noticeably larger (significant, $P < 0.01$) variability (std.) in canopy structure in terms of both density (ECC and ACC_{75}) and canopy level clumping (CI), than the other forest classes (primary, lightly logged,

twice logged forest, and salvage logged stage 1). Compared to all forest plots, oil palm canopy was more (significant, $P < 0.01$) open (lower values of all canopy structural variables) with the largest variation in cover, as well as having the most clumped canopy (lowest mean CI). Comparing the canopy structural variables, vertical cover was more variable than hemispherically-integrated cover. That is, for different forest classes ECC had higher coefficient of variation (CV = 5.5 – 45.1%) than ACC_{75} (CV = 0.7 – 31.2%). LAI in turn varied more than ACC_{75}. That is, CV of LAI_{eff} was higher by 3.8 – 13.6% than ACC_{75}, while CV of LAI_{true} was higher by 4.0 – 9.4% than ACC_{75}.

Table 5. Mean canopy structural variables (standard deviation in parentheses) derived from hemispherical photos: effective canopy cover (ECC), angular canopy closure 0 – 75° (ACC_{75}), effective leaf area index (LAI_{eff}), canopy clumping index (CI) and true leaf area index (LAI_{true}).

Forest classes	No. of plots	ECC %	ACC_{75} %	LAI_{eff}	CI	LAI_{true}
Primary forest	5	84.9 (4.7)	90.5 (0.7)	2.88 (0.13)	0.87 (0.02)	3.32 (0.15)
Lightly logged forest	8	85.7 (2.4)	90.9 (2.4)	2.99 (0.36)	0.83 (0.03)	3.60 (0.43)
Twice-logged forest	13	85.4 (5.4)	90.9 (1.9)	2.97 (0.23)	0.85 (0.03)	3.48 (0.23)
Salvage logged forest stage 1	26	80.8 (7.0)	88.0 (2.7)	2.65 (0.28)	0.82 (0.03)	3.25 (0.34)
Salvage logged forest stage 2	23	67.1 (18.0)	79.9 (11.4)	2.25 (0.53)	0.72 (0.11)	3.04 (0.49)
Oil palm plantation	13	52.1 (23.5)	60.3 (18.8)	1.42 (0.64)	0.64 (0.14)	2.00 (0.64)
All	88	74.3 (17.7)	82.6 (13.8)	2.45 (0.65)	0.77 (0.11)	3.08 (0.64)

Next, we examined more closely how the canopy gap fraction was distributed in different view zenith angles. Overall, directional canopy gap fraction tends to decrease with view zenith angle, being the highest in nadir direction (Figure 4). Salvage logged stage 2 and oil palm showed more variable directional gap fraction. Directional gap fraction also tends to decrease in variability towards horizon (or, in other words, the larger the mean gap fraction, the larger its

variability, in absolute term), with the exception of oil palm which showed relatively smaller decrease in canopy gap fraction variability across zenith angles.

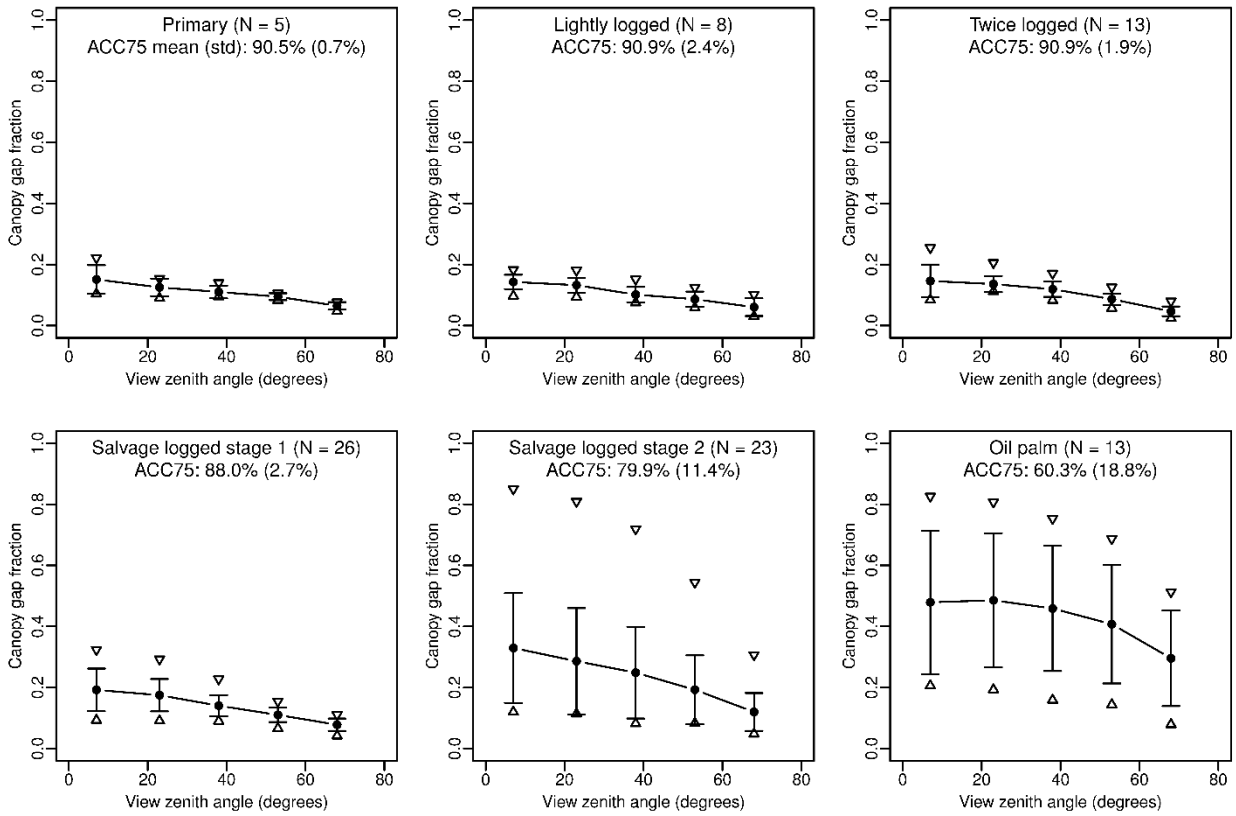

Figure 4. Angular profile of canopy gap fraction calculated from hemispherical photos. ACC_{75} is angular canopy closure 0 – 75°. Filled circles are the mean. Error bars represent one standard deviation. The lower triangles are minimum, the upper triangles maximum values.

To better appreciate the angular dependency, we calculated the shape function (Figure 5), which is defined as the normalized value of the canopy light extinction coefficient at a given zenith angle (Rautiainen and Stenberg, 2015). The shape function is based on the modified Beer's law equation so that the extinction coefficient is equal the product of mean projection of unit foliage area $G(\theta)$ and the directional clumping index $\beta(\theta)$. Variation in the shape function is induced by differences in leaf orientation and directional clumping indices. Similar angular pattern in the shape function was observed for primary, lightly logged, twice logged, and salvage logged

stage 1 plots; small decrease in shape function from the first (0 – 15°) to second (15 – 30°) zenith rings (note that sun zenith angle at Landsat overpass is 27 – 38°, Table 2), followed by progressively larger shape function decrease towards the horizon. In contrast, the angular shape function profile of salvage logged stage 2 and oil palm appeared to differ from the rest. Second and third (30 – 45°) ring shape function remained as high or was higher than vertical gap fraction in salvage logged stage 2 plots. Oil palm plots showed somewhat linear trend of shape function decrease as a function of view zenith angles. Shape functions of all vegetation types converged near horizon.

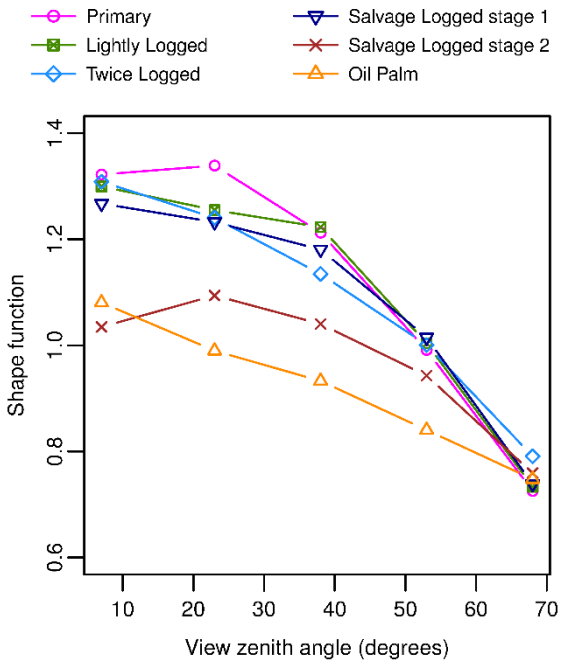

Figure 5. Average shape function, defined as the normalized value of the canopy light extinction coefficient at a given zenith angle for all forest classes. Calculated from hemispherical photos.

Plot-wise relationship between derived canopy structural variables (Figure 6) showed that for the same vertical cover (ECC), oil palm consistently had lower LAI_{true} (Figure 6a) and ACC_{75} (Figure 6b). For the same LAI_{true}, salvage logged stage 2 plots had lower ECC. ECC increased with LAI_{true} up to when LAI_{true} reached around 3, beyond which ECC stayed below ~92% whereas LAI_{true} continued to increase up to more than 4. Similarly ACC_{75} showed an asymptote

at ~93%. For all plots, ECC was usually lower than ACC_{75}. The bidirectional gap probability in the sun and sensor direction showed that sunlit ground visibility largely diminished at LAI_{true} approximately 3 (Figure 6d).

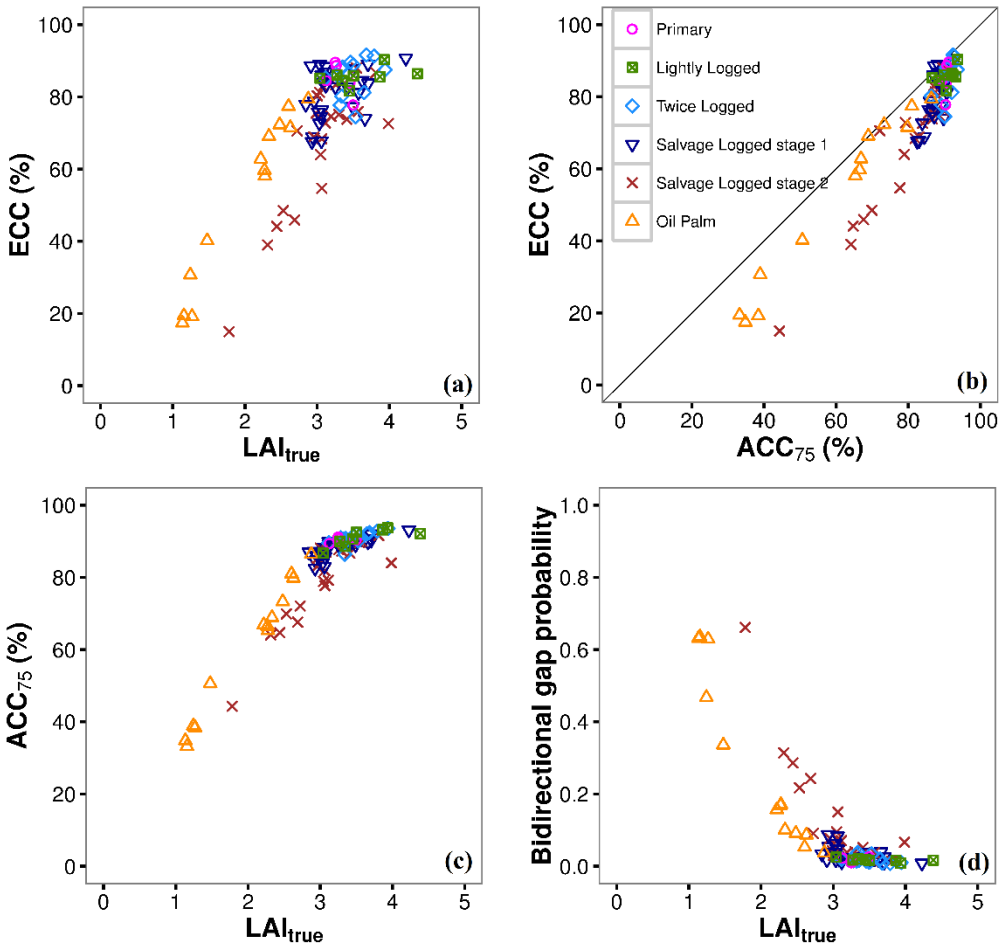

Figure 6. Relationship between canopy structural variables. (a) Effective canopy cover (ECC) and true leaf area index (LAI_{true}). (b) ECC and angular canopy closure 0 – 75° (ACC_{75}). (c) ACC_{75} and LAI_{true}. (d) Bidirectional gap probability and LAI_{true}. Bidirectional gap probability is calculated from canopy gap fraction in sun illumination and sensor view direction ($cgf(\theta_{view}) \times cgf(\theta_{sun})$).

3.2. Satellite BRF response to canopy structure

Even after filtering pixels based on atmosphere opacity (haziness), very weak negative relationship ($r < 0.3$) was observed between ETM+ BRF and canopy structural variables for forest plots (Figure 7, Table 6). Sample size was deemed not adequate for assessing correlation by forest class. Moderate negative correlation ($r > 0.7$) was observed for oil palm plots (slightly higher with LAI_{true} than with ECC), except in near-infrared. Looking at spectral differences between forest classes while considering canopy density, oil palm plots were brighter in red and shortwave-infrared, and at the same ECC, brighter than salvage logged stage 2. Among the forest plots, salvage logged stage 2 plots (which were being converted to fragmented agriculture) were brighter despite having similar ECC and LAI_{true}. Lightly logged plots were slightly darker in near-infrared and shortwave-infrared. Spectral vegetation indices did not correlate with ECC or LAI_{true} better than individual band (Table A1 Appendix A).

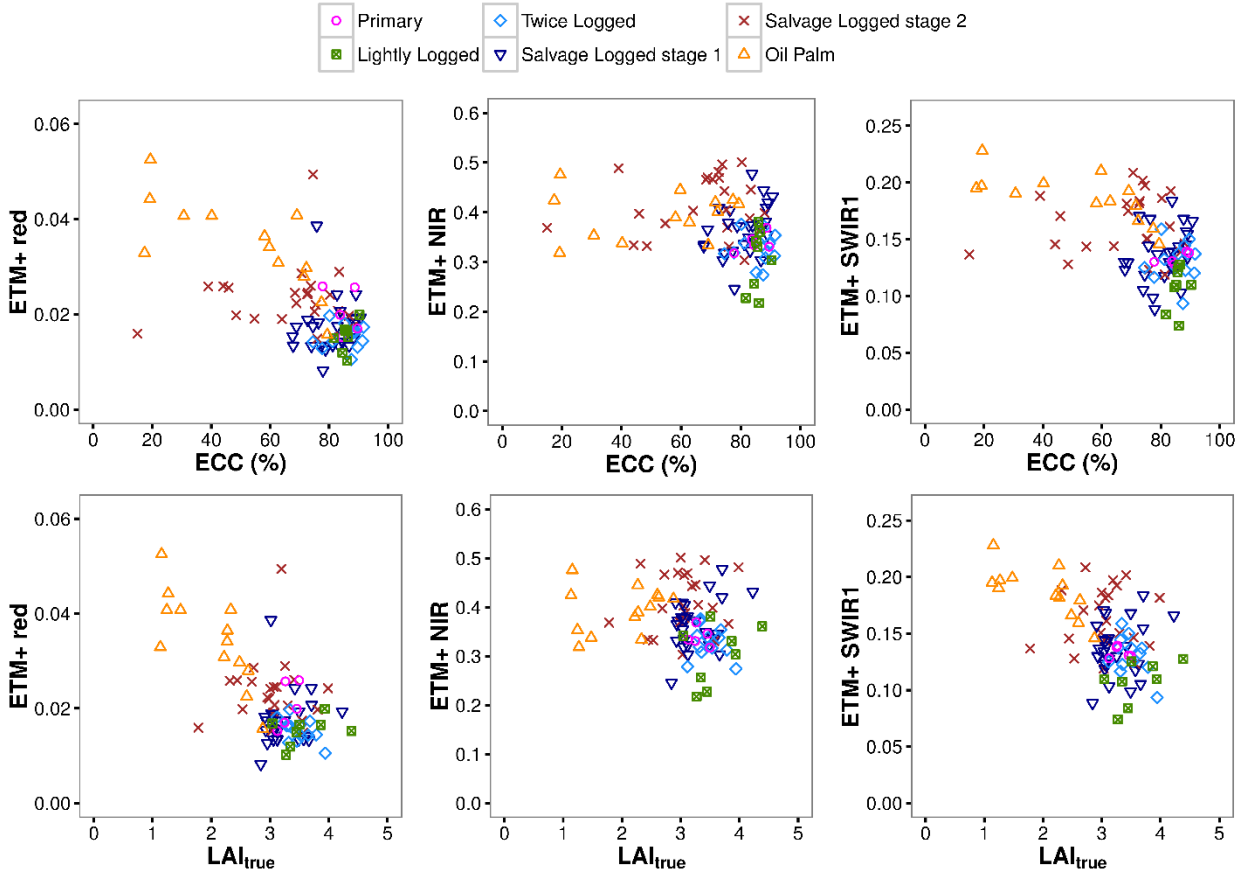

511 Figure 7. Landsat-7 ETM+ surface reflectance (BRF) response to effective canopy cover (ECC)
512 and true leaf area index (LAI_{true}).
513
514 Table 6. Correlation coefficient between satellite BRF and true leaf area index (LAI_{true}) or
515 effective canopy cover (ECC).

Forest classes	BRF vs. LAI_{true}					BRF vs. ECC				
	green	red	NIR	SWIR1	SWIR2	green	red	NIR	SWIR1	SWIR2
All forests (N = 75)	-0.18	-0.17	-0.12	-0.19	-0.21	-0.29	-0.23	-0.21	-0.22	-0.22
Oil palm (N = 13)	-0.75	-0.77	0.19	-0.72	-0.78	-0.72	-0.74	0.12	-0.72	-0.76

516
517
518 **3.3. Forest BRF simulation and validation**
519 We focused the BRF modelling on closed-canopy forests i.e., excluding oil palm, and salvage
520 logged forest stage 2 which structurally resembles more agricultural land. In our first forest
521 BRF simulations with PARAS model, we fixed leaf albedo (i.e. PROSPECT simulations were
522 based on mean leaf constituents), and thus, forest BRF was driven by solely canopy structure.
523 The modelled BRF showed lack of variability in near-infrared and shortwave-infrared, as
524 compared to in visible domain (Figure 8). Overall the levels of the modelled BRF were within
525 the range of observed satellite BRF. Concerning overall BRF levels, PARAS simulations
526 underestimated green BRF (mean difference MD -24.2%) and overestimated SWIR1 BRF (MD
527 23.8%), with closer level to observed ETM+ in NIR (MD 2%) and red (Table 7). All plots
528 considered, relative RMSD was largest in red band (65%), smallest in NIR (16%), and moderate
529 in green and SWIR1 (30-36%). In the red domain where the level and variability best matched
530 ETM+-observed BRF (Figure 8), a number of salvage logged plots had their BRF
531 overestimated, causing larger overall error than other forest classes. Overall, no apparent

differences in the agreement between modelled and observed BRF between forest classes were observed (Figure 8).

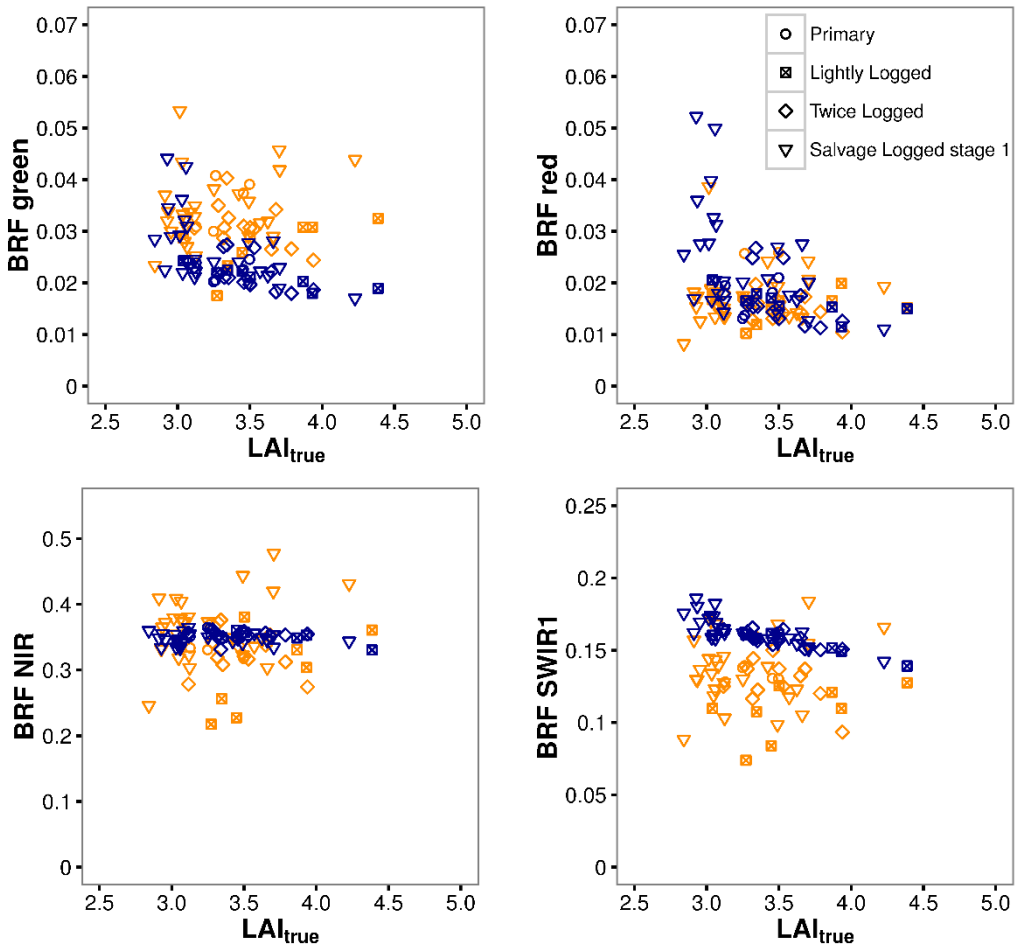

Figure 8. Comparison of modelled BRF (leaf albedo fixed to PROSPECT simulation with mean *Dipterocarpaceae* family leaf constituents) to measured Landsat-7 ETM+ surface reflectance, with respect to true leaf area index (LAI_{true}). PARAS-modelled BRFs are shown in blue, ETM+-observed BRFs in orange.

Table 7. PARAS-modelled BRF vs. Landsat-7 ETM+ BRF for closed-canopy forest plots (N = 52; all forest plots excluding salvage logged stage 2). In parentheses are relative (%) to average ETM+ BRF (Mean ETM+). MD is modelled minus observed value. RMSDC is root mean

544 squared differences corrected for bias (MD). Results for each forest class are shown in Table
545 A2 Appendix A.

546

Band	Mean ETM+	Mean PARAS	Std ETM+	Std PARAS	RMSD	MD	RMSDC
Green	0.033	0.024	0.006	0.006	0.012 (36.4)	-0.008 (-24.2)	0.008 (24.2)
Red	0.017	0.021	0.005	0.009	0.011 (64.7)	0.004 (23.5)	0.010 (58.8)
NIR	0.343	0.350	0.051	0.009	0.054 (15.7)	0.007 (2.0)	0.054 (15.7)
SWIR1	0.130	0.161	0.022	0.009	0.040 (30.8)	0.031 (23.8)	0.025 (19.2)

547

548

549 In our second set of forest BRF simulations with PARAS model, leaf albedo was not fixed.
550 Structural variables were parameterized based on field measurements as in the first set of
551 simulations. Varying leaf constituents produced larger variability in leaf albedo (ω_L) in green
552 and SWIR, whilst relatively smaller variability in red and NIR (Figure 9). At the canopy level,
553 this ω_L variability produced BRF variability of similar magnitude to variability observed in
554 satellite BRF in green and SWIR, whilst variability in NIR from other sources remained
555 unaccounted (Figure 10). Leaf albedo variation affected red BRF the least.

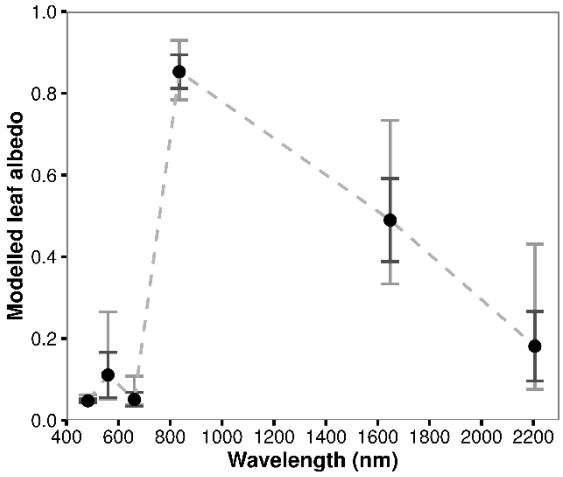

Figure 9. Variability in modelled leaf albedo of *Dipterocarpaceae* family. Points show the mean of the 2500 PROSPECT simulations, black error bar shows the one standard deviation, and grey error bar shows the minimum and maximum.

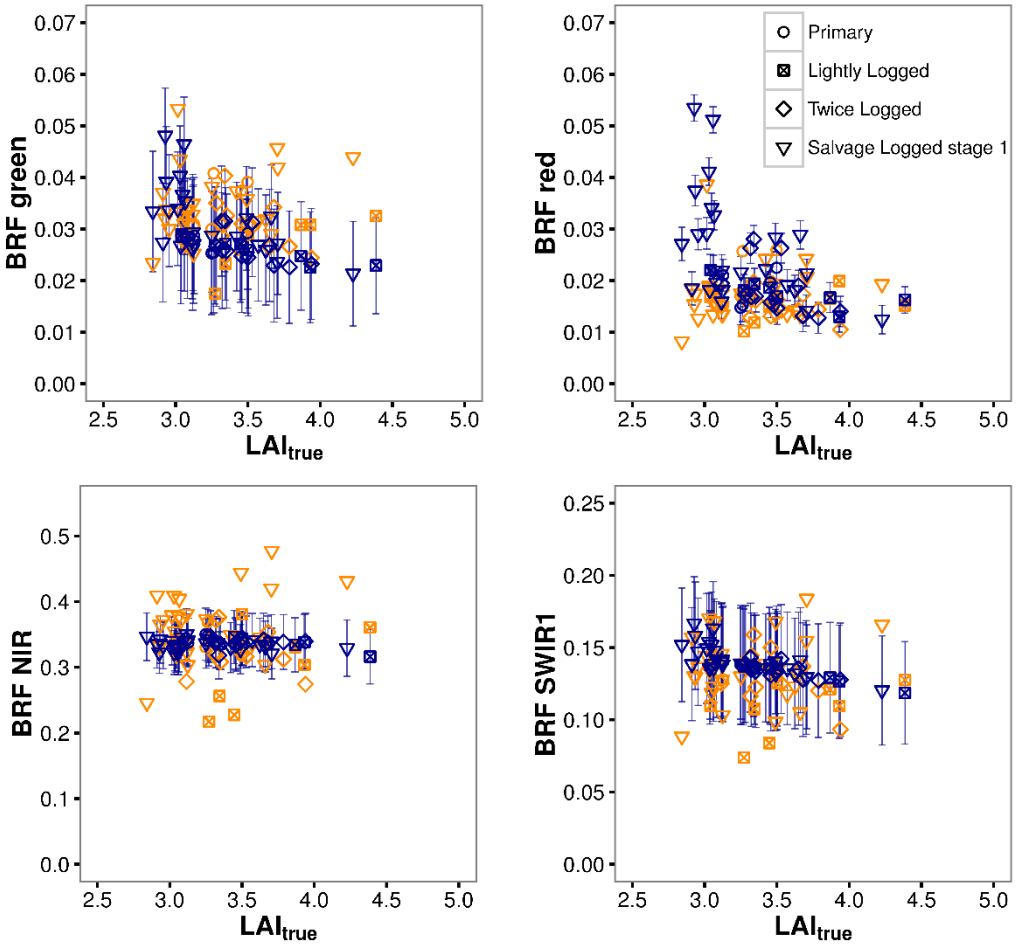

Figure 10. Variability (std) in PARAS-modelled BRF resulting from variability in leaf albedo (Figure 9, range from minimum to maximum), and comparison to observed Landsat ETM+ BRF variability, with respect to true leaf area index (LAI_{true}). PARAS-modelled BRFs are shown in blue, ETM+-observed BRFs in orange.

3.4. Global sensitivity analysis: drivers of canopy BRF

Based on the range of measured canopy structural variables (LAI_{eff} 2.17 – 3.48, i_0 0.73 – 0.92, cgf(θ_{view}) 0.08 – 0.32), leaf albedo was found to provide the dominant, largest contribution (> 80%, Figure 11a) to canopy BRF across the optical domain (even with the smaller one standard deviation of simulated leaf albedo i.e., > 50% contribution, Figure 11b). The only exception was in the red band where BRF was most sensitive to canopy gap fraction in sensor view direction (nadir view i.e., 0 – 15°). BRF was more sensitive to directional gap fraction than

hemispherically-integrated cover measures (such as effective LAI). Ground contribution was negligible.

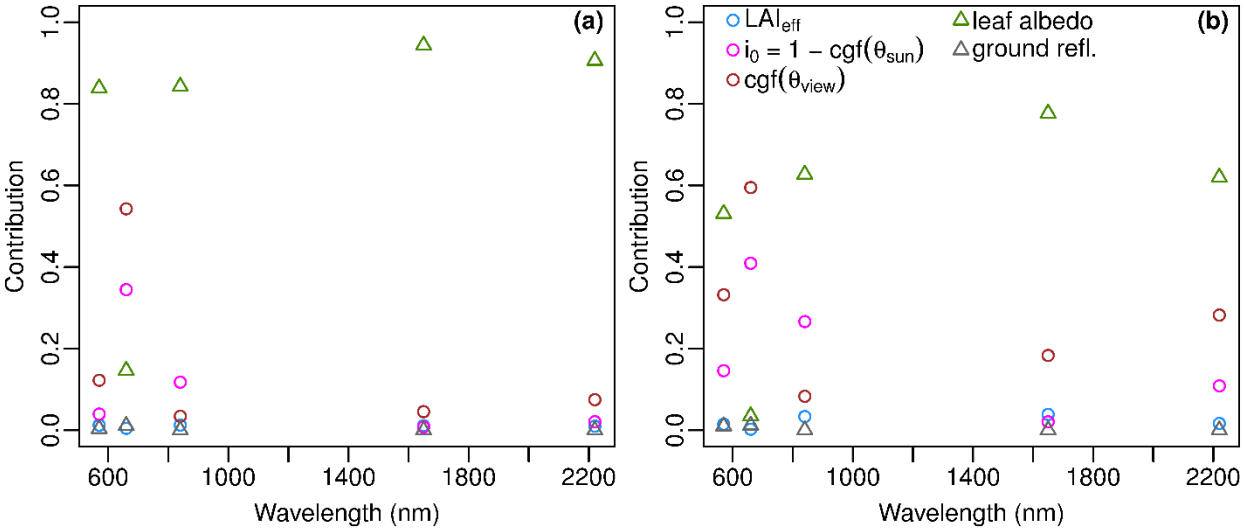

Figure 11. Global sensitivity analysis of PARAS BRF model in closed-canopy humid tropical forests (primary, lightly logged, twice logged, salvage logged stage 1). BRFs were modelled in ETM+ green, red, NIR, SWIR1, and SWIR2 channels. Relative contribution was measured with sobol total effect indices. (a) is based on maximum range of leaf albedo (Figure 9), (b) based on one standard deviation of leaf albedo.

Finally, we tested changing the model inputs one at a time to identify possible ways to improve the agreement between modelled and measured BRF (Table A3 Appendix A). Compared to base case simulation, across the spectral bands, modelled BRF was most sensitive to changes in p (0.735 ± 0.020 for the modelled closed-canopy). Overall, none of the tested input change brought improvements in PARAS agreement to ETM+-observed BRF across all spectral bands.

4. Discussion

We observed differences in canopy structure between the less degraded forests (lightly-logged, twice-logged, salvage logged stage 1), and the more degraded salvage logged stage 2 and oil

palm plots (Table 5, Figure 4, 5). The less degraded forests, on the other hand, were structurally similar to undisturbed primary forests, indicating that the canopy structure has possibly recovered to pre-disturbance condition. However, whether it was also the case for plant communities remains an open question. They possessed similar total cover (ECC, LAI), as well as similar angular profiles of gap fractions, which was characterized by (1) largest gap fraction near zenith, and (2) decreasing gap fraction and gap fraction variability with view zenith angle towards the horizon. The gap concentration near the zenith where solar radiation flux is the highest at the equator, and less concentrated gaps near horizon (i.e., mid-height in the canopy) where light penetration is low had also been observed by Trichon et al. (1998) in Central Sumatera, Indonesia. The pattern of decreasing variance of gap fraction with view zenith angle is in agreement to theoretical results in Ryu et al. (2010). It is also interesting to note that this angular profile differs from other biomes such as the generally sparser boreal forests (Rautiainen and Stenberg, 2015) which resemble more salvage logged stage 2 forest profile in our data, featuring more or equal gaps in second and third zenith annulus (up to 45°) as in nadir direction (Figure 5). In contrast to the forest plots, oil palm featured highly variable gap fraction across zenith angles (gaps can be found in all directions in the canopy, Figure A1 Appendix A), which resulted in lower LAI at the same vertical cover (ECC, Figure 6a). Structurally, the oil palm canopy appeared different from the most open forest class (i.e., salvage logged stage 2) at the same total cover. The more dispersed and variable gaps across zenith angles in oil palm canopy is expected in typical managed plantations where exclusion distances among trees are larger than in natural forests (Geng et al., 2016). From the remote sensing perspective, sunlit forest floor visibility to nadir-viewing sensor greatly diminished at LAI_{true} around 3 (Figure 6d), beyond which ground impact on canopy-level reflectance therefore likely became negligible.

615 The satellite data showed overlap in BRFs between forests with similar canopy structure i.e.,
616 primary, lightly logged, twice logged, and salvage logged stage 1 (Figure 7). The values of
617 photon recollision probability *p* were indeed similar for these forest classes i.e., 0.73 ± 0.012
618 (primary), 0.746 ± 0.024 (lightly logged), 0.740 ± 0.014 (twice logged), and 0.729 ± 0.020
619 (salvage logged stage 1). The more degraded salvage logged stage 2 was, however, brighter
620 than other forest classes, as well as was spectrally separable (in red and SWIR) from the
621 brightest oil palm plots at the same canopy cover. The former may have been due to the higher
622 gap probability in solar illumination direction at satellite overpass time (sun zenith angle 27–
623 38° i.e., between second and third ring. The oil palm plots were (except 2 plots) younger than
624 10 years old (planted in 2006) which corresponds to the age when Malaysian oil palm leaf area
625 stabilizes (McMorrow, 2001). Stronger response of satellite BRF to forest aboveground
626 biomass than oil palm had similarly been observed by Morel et al. (2012). They attributed it to
627 the simpler canopy structure of oil palm monoculture in which increasing canopy closure
628 increases shade fraction over the relatively bright ground cover. The flat relation between near-
629 infrared BRF and canopy cover is likely due to the undergrowth in young oil palm plots
630 typically colonized by weeds or sown legumes (McMorrow, 1995). The high species diversity
631 (and thus high variation in leaf biochemical signature) in the tropical forest plots also likely
632 partly explained the low correlation for forest plots as they induced large BRF variability at
633 canopy level (Figure 10).
634
635 Based on our results, the green and SWIR appeared to be optimal spectral bands to detect leaf
636 biochemical (and in turn, potentially tree species) diversity from satellite BRF (Figure 10). That
637 is, in green and SWIR, variations in observed canopy BRFs can be largely attributed to
638 variations in leaf albedo. Based on measured leaf spectra and canopy structural variables from
639 literature, Asner et al. (2012, Figure 6D) similarly showed for the *Dipterocarpaceae* family,

coefficients of variation in canopy BRF is higher in SWIR (~16-20%) and green (~12%) as compared to in red (~7%) and NIR (~6%). In NIR, publicly available leaf spectral measurements showed that, unlike in other spectral domains, leaf reflectance and transmittance are negatively correlated (*r*: -0.77, based on the published leaf spectra for Sycamore maple, the dominant broadleaved species in ANGERS database, Feret et al., 2008), which may have suppressed variability in leaf NIR single-scattering albedo (= reflectance + transmittance). Asner et al. (2012) noted the range of C_m, the leaf constituent that mainly drives leaf NIR albedo, for the Bornean lowland tropical species is nearly equal to the range found for global humid tropical forests and other biomes. This further suggests that the limited expression of leaf constituents in NIR BRF of dense canopies applies similarly across vegetation types. C_m also does not strongly co-vary with C_{ab} (*r*: 0.19) or C_w (*r*: 0.63) based on global vegetation dataset as reported by Feret et al. (2011b). In red, the relatively much higher photosynthetic pigment content in leaves of *Dipterocarpaceae* family (mean C_{ab} 75.09 μg cm^{-2})—as compared to the global mean of various vegetation types (32.81 μg cm^{-2}, Feret et al., 2011b)—causes relatively lower mean and variability (in absolute term) of leaf albedo in red, where C_{ab} absorbs the strongest. The pigment absorption is not as strong in green. Large variability in SWIR BRF is mainly driven by C_w variability (Jacquemoud et al., 2009).

We modelled BRF focusing on closed-canopy humid tropical forest (undisturbed primary, and forests with subtle degradation i.e., lightly logged, twice logged, salvage logged stage 1), excluding oil palm, and salvage logged stage 2 which structurally resembled less of a forest but more of agriculture landscape. In doing so the impact of uncertainty in ground surface cover and reflectance (which is expected to vary with canopy openness in light-abundant tropical environment) was additionally minimized. Indeed, salvage logged plots with lower LAI had their red BRF overestimated (Figure 8, 10), likely indicating the presence of understory

665 vegetation (which would have lower red reflectance) underneath not-recent canopy gaps. This
666 potentially complicates identification of degraded forests based on spectrally unmixed soil
667 fractions, and calls for studies monitoring the succession of understory vegetation (ginger,
668 shrubs, ferns, grasses, palms) post-disturbance. Concerning the modelled BRF, Rautiainen and
669 Stenberg (2005) applied PARAS BRF parameterization in boreal forest and obtained absolute
670 RMSD against Landsat ETM+ of 0.009 – 0.010 in red and 0.040 – 0.049 in near-infrared, which
671 is close to RMSD in our study (0.011 in red, 0.054 in NIR). To note is that the RMSD measures
672 the combined uncertainty in modelled BRF, as well as uncertainty in the ETM+ surface
673 reflectance (SR) which is expected to be within 5%×SR+0.005 (Claverie et al., 2015). Further
674 PARAS applications and hemispherical photos acquisitions in different forest areas in the
675 tropics, as well as in different forest biomes are encouraged to evaluate the generality of the
676 PARAS performance.
677
678 The global (as opposed to local, one-factor-at-at-time) sensitivity analysis we performed
679 (Figure 11) revealed the leaf optical properties control dominantly BRF in Bornean closed-
680 canopy humid tropical forests. This supports the assertion that dense (tropical) forests are good
681 candidates for retrievals of foliar and canopy biochemistry using remote sensing (Asner, 1998;
682 Baret et al., 1994). In other words, the assumption that the closed-canopy humid tropical forests
683 are optically thick was not violated based on our findings. Our results showed leaf single
684 scattering albedo was strongly expressed at the canopy level in all ETM+ bands, with the
685 exception of highly absorbing red domain where variability in leaf constituents produced the
686 smallest variability in leaf albedo as modelled by PROSPECT. Leaf optics contributed the most
687 to canopy BRF in shortwave infrared, driven by large variability in leaf water content. Whereas
688 canopy structure has been parameterized based on measurements, we acknowledge the
689 uncertainty in PROSPECT-estimated leaf albedo variability. Nevertheless, we showed the

690 reduced, but still dominant (from > 80% to > 50% BRF contribution) role of leaf optical
691 properties when we applied one standard deviation of modelled leaf albedo, instead of the
692 modelled full range. However, we note that in the NIR domain, the observed BRF variability
693 was not entirely produced by variability in canopy structure and leaf albedo based on our
694 modelling results. The remaining variability in NIR BRF can originate from unaccounted
695 canopy structure influence on NIR BRF, or from the underestimation of leaf albedo variability
696 in NIR. Studies from the Amazon (e.g., Samanta et al., 2012) suggest the impact of epiphylls
697 growth and film of water which coat the surface of leaves, as well as leaf shedding and flushing
698 mechanisms, on leaf NIR albedo (the latter may also change total leaf area and thus photon
699 recollision probability *p*). In the red band, and when leaf optics decreased in their influence on
700 canopy BRF due to lower leaf albedo variability, canopy gap fraction in sensor view direction
701 was the most important canopy structural property. More generally, the directional gap fraction
702 was shown to be more influential than the total, hemispherically-integrated tree cover (i.e.,
703 LAI). Asner and Martin (2008) similarly demonstrated minimal effect of random variation in
704 LAI (3.0–6.5) on leaf biochemical signal propagation to canopy level in Australian rainforest.
705 This serves to emphasize the importance of accounting for foliage clumping (which determines
706 angular distribution of canopy gaps) in characterizing the canopy radiative transfer, indicating
707 the severe limitation of models which represent the canopy as a turbid medium in humid tropical
708 forests.
709
710 Despite our best efforts in providing ecologically realistic range of the inputs—on which results
711 of sensitivity analysis are dependent—used in the BRF models, the difficulty, and consequently
712 lack of available spectral measurements in humid tropical forest of South East Asia caused
713 unavoidable uncertainties in our modelling experiments. Modelled leaf albedo in this study
714 relied on reliable leaf constituents and accuracy of PROSPECT model; our test applying the

bias reported in Feret et al. (2008) for tropical Hawaii dataset showed minimal impact of the bias on canopy BRF (Table A3 Appendix A). We also tested varying the N mesophyll structure parameter (1.7 – 2.5 for Dicotyledons leaves based on Jacquemoud and Baret, 1990), which produced similar range of leaf albedo (reflectance + transmittance) as when N was fixed in this study. The forthcoming release of Spectranomics database of tropical leaf spectral-chemical libraries (Asner and Martin, 2016; https://cao.carnegiescience.edu/spectranomics) combined with our canopy structural measurements will allow further verification of our findings, as well as modelling for the oil palm (monocotyledonous) tree crop (*Elaeis guineensis*) currently not possible. In the latter, one needs to consider the different optical properties (and likely biochemical composition) of leaves from young oil palm recently transferred from nursery (i.e. seedling, which is often used in controlled experiment e.g., water treatment), and leaves from the mature oil palm tree (Ritchie and Runcie, 2014).

Concerning the PARAS model (Table 3), the *p* estimation depends on the reliable ratio between diffuse non-interceptance (DIFN) and true leaf area index (LAI_{true} = LAI_{eff} / CI). LAI_{eff} (CI) was estimated from gap fraction (gap size distribution) derived from the hemispherical photos, which was subject to uncertainties caused by image acquisition (sampling, weather, exposure) and automatic thresholding steps. ECC estimation was also probably less than ideal with only 12 photos per plot (Korhonen and Heikkinen, 2009). Ideally, complementary LAI measurements with LAI-2000 would allow evaluating the accuracy of estimated LAI_{eff}, while LAI_{true} could be measured by litter trap or direct leaf harvest sampling. Operating LAI-2000 which requires taking sky irradiance readings from above the canopy (or in sufficiently large clearing area) would, however, be impractical in our studied dense and tall tropical forest. Harvesting leaves (and woody elements for wood area correction) from the tall canopy, for many sample plots, would also require enormous efforts, not possible without tower platform,

in this ecosystem. Nevertheless, clumping index estimated in this study for closed-canopy forests i.e., 0.74 – 0.88 is close to the only available estimate in old-growth tropical rainforest in Costa Rica i.e., 0.71 – 0.82 (Olivas et al., 2013). A test (Table A3 Appendix A) of incorporating 11% woody element (from total plant area) based on direct harvest in the same study and woody stem reflectance from Asner (1998) showed relatively minor influence on our simulated BRF. Asner (1998) similarly found minor role of stem area index in Brazilian tropical woodlands (LAI 3.1 – 5.9). Replacing soil with darker litter reflectance in tested spectra decreased RMSD in red (which was most sensitive to vertical gap and thus ground visibility to sensor) because it reduced the modelled BRF for the overestimated salvage-logged plots (Figure 8, 10). Overall our experiments from Table A3 (Appendix A) indicated that improving PARAS BRF agreement to the observed ETM+ BRF requires mainly adjustment of spectral inputs.

Summarizing, the physically-based forest reflectance interpretation presented in this study offers insights into the limitations, but also opportunities in how well optical Earth observation data from operational Landsat-class satellites can be used to uncover structural variation along a gradient of forest degradation in humid tropical forests. On one hand, our findings showed the limited capability of optical remote sensing in revealing the full forest structural variation (i.e., difficulty in discriminating the less intensively logged forests from primary forests due to canopy structure similarity) of forest landscapes in this region with predominant human modification. On the other hand, the findings indicated high feasibility to retrieve leaf optical properties, and in turn leaf biochemistry, from the observable top-of-canopy reflectance. In another perspective, this implied accounting for the variability in leaf optical properties would improve optical data interpretation (and inversion e.g., LAI retrieval) in this biome, thus calling for synergistic efforts in ground measurements of both forest structure and leaf optical properties.

5. Conclusions

We presented the first application of the spectral invariants theory in modeling the reflectance of humid tropical forests. In doing so, we integrated field measurements of canopy structure from insular Southeast Asia, coupled leaf-level PROSPECT and canopy-level PARAS model, and concurrent satellite observations. The analysis was done within the context of the operational Landsat-class spatial and spectral resolution. Close examination of canopy structure showed structural similarity between the closed-canopy forests which were undisturbed (primary), lightly logged, twice logged, and salvage logged (stage 1). Consequently, canopy reflectance observed by Landsat-class satellite was not sensitive to these different degrees of degradation. The more degraded salvage logged stage 2, and oil palm were however potentially distinguishable. This structure-induced BRF "saturation" (i.e., weak correlation between BRF and canopy structural variables) however potentially provides advantage for foliage and canopy chemistry sensing in closed-canopy humid tropical forests: global sensitivity analysis revealed the dominant contribution of leaf optical properties to canopy-level BRF in green and shortwave infrared domain. The strongly absorbed red band on the other hand was most sensitive to (vertical) effective canopy cover. Directional gap fraction played a stronger role than hemispherically-integrated leaf area index in driving BRF response, indicating the importance of explicitly accounting for foliage clumping. Further studies are needed concerning the salvage logged stage 2 and oil palm plots characterized by large canopy openings, requiring measurements of forest floor cover and reflectance in stands of varying canopy cover.

Acknowledgements

We thank the two anonymous reviewers for constructive comments. We thank Aarne Hovi for fruitful continuous discussions, Alemu Gonsamo for help with CIMES software, Bertrand Iooss

for discussion on global sensitivity analysis, Mait Lang for help during processing of hemispherical photos, and all parties involved in the establishment and maintenance of the SAFE large-scale experimental forest fragmentation landscape. The Landsat-7 ETM+ images were courtesy of United States Geological Survey. This study was funded by Aalto University (grant 91160122).

Appendix A

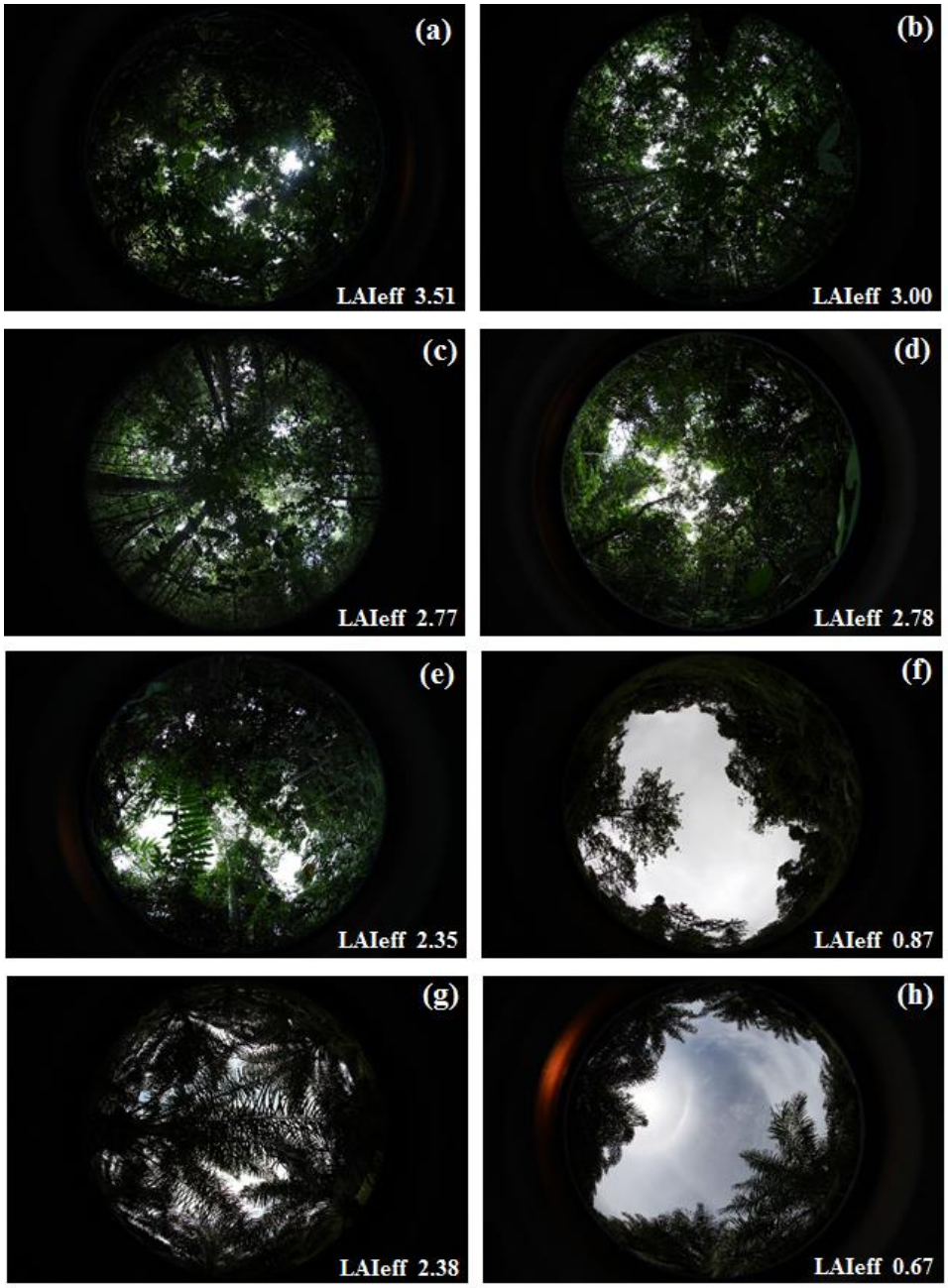

Figure A1. Example hemispherical photos of the different forest classes, and oil palm plantation. LAI_{eff} is effective leaf area index calculated for the respective photo. (a) Primary forest; (b) Lightly logged forest; (c) Twice logged forest; (d) Salvage logged forest stage 1; (e-f) Salvage logged forest stage 2; (g-h) Oil palm plantation.

Table A1. Correlation coefficient between spectral vegetation indices and true leaf area index (LAI_{true}) or effective canopy cover (ECC). NDVI = normalized difference vegetation index. EVI = enhanced vegetation index. NDMI = normalized difference moisture index. NBR = normalized burn ratio.

Forest classes	BRF vs. LAI_{true}				BRF vs. ECC			
	NDVI	EVI	NDMI	NBR	NDVI	EVI	NDMI	NBR
All forests (N = 75)	0.13	-0.10	0.22	0.22	0.15	-0.17	0.11	0.13
Oil palm (N = 13)	0.71	0.37	0.65	0.69	0.66	0.30	0.60	0.64

Formulas:

NDVI = (NIR - red) / (NIR + red) (Tucker, 1979)

$$EVI = 2.5 * \left(\frac{NIR - red}{NIR + (6 * red) - (7.5 * blue) + 1}\right)$$ (Huete et al., 2002)

NDMI = (NIR - SWIR1) / (NIR + SWIR1) (Gao, 1996)

NBR = (NIR - SWIR2) / (NIR + SWIR2) (Key and Benson, 2006)

Table A2. PARAS-modelled BRF vs. Landsat-7 ETM+ BRF for each closed-canopy forest class. In parentheses are relative (%) to average ETM+ BRF (Mean ETM+). MD is modelled minus observed value. RMSDC is root mean squared differences corrected for bias (MD).

Band	Primary (N = 5)			Lightly logged (N = 8)		
	RMSD	MD	RMSDC	RMSD	MD	RMSDC
Green	0.014 (38.9)	-0.013 (-36.1)	0.005 (13.9)	0.008 (29.6)	-0.006 (-22.2)	0.006 (22.2)
Red	0.006 (28.6)	-0.004 (-19.0)	0.005 (23.8)	0.005 (33.3)	0.001 (6.7)	0.004 (26.7)
NIR	0.025 (7.4)	0.018 (5.3)	0.017 (5.0)	0.079 (26.2)	0.047 (15.6)	0.063 (20.9)

SWIR1	0.029 (21.8)	0.028 (21.1)	0.005 (3.8)	0.053 (49.5)	0.048 (44.9)	0.023 (21.5)

Table A2 (cont.)

Band	Twice logged (N = 13)			Salvage logged stage 1 (N = 26)		
	RMSD	MD	RMSDC	RMSD	MD	RMSDC
Green	0.010 (32.3)	-0.009 (-29.0)	0.004 (12.9)	0.013 (38.2)	-0.008 (-23.5)	0.010 (29.4)
Red	0.005 (33.3)	0.002 (13.3)	0.005 (33.3)	0.014 (82.4)	0.007 (41.2)	0.012 (70.6)
NIR	0.042 (12.8)	0.025 (7.6)	0.034 (10.4)	0.055 (15.1)	-0.017 (-4.7)	0.052 (14.2)
SWIR1	0.032 (24.4)	0.027 (20.6)	0.016 (12.2)	0.040 (29.4)	0.028 (20.6)	0.028 (20.6)

Table A3. Changes in PARAS-modelled BRF and its agreement to ETM+-observed BRF due to change in specific model input (see Table 3 for model input description). (a) Relative MD is mean difference between BRF modelled with the specific input change, and BRF modelled in base case simulation (Figure 8, Table 7), as percentage from mean base case simulation. (b) Absolute change in relative RMSD (PARAS vs. ETM+, relative to mean ETM+ BRF) i.e., rel. $RMSD_{input\_changed}$ minus rel. $RMSD_{base\_case}$ (negative value means improved agreement).

Input changed	(a) Relative MD (input - Δ% / input + Δ%)				(b) Δ relative RMSD (input - Δ% / input + Δ%)			
	green	red	NIR	SWIR1	green	red	NIR	SWIR1
LAI_{true} ± 20%	+12.5 / -8.3	+4.8 / -4.8	+5.4 / -4.9	+11.8 / -8.7	-6.1 / +3.0	0.0 / -5.9	+1.8 / +0.3	+12.3 / -7.7
p ± 20%	+33.3 / -33.3	+19.0 / -19.0	+19.1 / -33.7	+34.8 / -44.1	-12.2 / +21.2	+5.9 / -5.9	+11.1 / +21.0	+38.4 / +6.9
p ± 10%	+16.7 / -16.7	+9.5 / -9.5	+10.6 / -14.0	+18.6 / -20.5	-9.1 / +9.1	0.0 / -5.9	+4.7 / +4.4	+19.2 / -10.8
Q ± 20%	-12.5 / +12.5	-4.8 / +4.8	-19.1 / +19.1	-17.4 / +17.4	+6.0 / -6.1	-5.9 / 0.0	+7.6 / +11.1	-11.6 / +18.4
ω_L ± 20%	-12.5 / +12.5	-4.8 / +4.8	-36.6 / +73.4	-24.8 / +32.3	+6.0 / -6.1	-5.9 / 0.0	+23.1 / +63.0	-10.8 / +35.4
Wood * = 11%	+4.2	+9.5	-16.3	-3.1	-3.1	+5.9	+5.6	-3.1
ρ_{ground} = litter **	-4.2	-9.5	-0.3	-3.7	0.0	-11.8	0.0	-3.9
ω_L = 40% liana ***	0.0	0.0	+2.9	+2.5	0.0	0.0	+0.6	+2.3
ω_L with PROSPECT bias ****	+4.2	+4.8	+5.7	+7.5	-3.1	0.0	+1.8	+7.7

* % wood area relative to total plant area measured by direct harvest in old growth tropical rain forest (plant area index 5.95), Central America (Olivas et al., 2013). Woody stem reflectance obtained from Asner (1998, Figure 2B).

** litter reflectance obtained from Asner (1998, Figure 2A).

*** modelled with PROSPECT-4 based on liana mean leaf constituents in Asner et al. (2012).

**** PROSPECT-4 bias in modelling tropical Hawaii leaf reflectance and transmittance reported in Feret et al. (2008).

References

Asner, G.P., 2000. A hyperspectral photon transport system for simulating imaging spectrometer observations of terrestrial ecosystems, in: Green, R.O. (Ed.), 9th Annual Airborne Earth Science Workshop. Jet Propulsion Laboratory, Pasadena, CA, pp. 126–138.

Asner, G.P., 1998. Biophysical and Biochemical Sources of Variability in Canopy Reflectance. Remote Sens. Environ. 253, 234–253.

Asner, G.P., Martin, R.E., 2016. Spectranomics: Emerging science and conservation opportunities at the interface of biodiversity and remote sensing. Glob. Ecol. Conserv. 8, 212–219.

Asner, G.P., Martin, R.E., 2008. Spectral and chemical analysis of tropical forests: Scaling from leaf to canopy levels. Remote Sens. Environ. 112, 3958–3970.

Asner, G.P., Martin, R.E., Suhaili, A. Bin, 2012. Sources of Canopy Chemical and Spectral Diversity in Lowland Bornean Forest. Ecosystems 15, 504–517.

Avitabile, V., Herold, M., Heuvelink, G.B.M., Lewis, S.L., Phillips, O.L., Asner, G.P., Armston, J., Ashton, P.S., Banin, L., Bayol, N., Berry, N.J., Boeckx, P., de Jong, B.H.J., Devries, B., Girardin, C.A.J., Kearsley, E., Lindsell, J.A., Lopez-Gonzalez, G., Lucas, R., Malhi, Y., Morel, A., Mitchard, E.T.A., Nagy, L., Qie, L., Quinones, M.J., Ryan, C.M., Ferry, S.J.W., Sunderland, T., Laurin, G.V., Gatti, R.C., Valentini, R., Verbeeck, H., Wijaya, A., Willcock, S., 2016. An integrated pan-tropical biomass map using multiple reference datasets. Glob. Chang. Biol. 22, 1406–1420.

Baret, F., Vanderbilt, V.C., Steven, M.D., Jacquemoud, S., 1994. Use of spectral analogy to evaluate canopy reflectance sensitivity to leaf optical properties. Remote Sens. Environ. 48, 253–260.

Baret, F., Weiss, M., Lacaze, R., Camacho, F., Makhmara, H., Pacholcyzk, P., Smets, B., 2013. GEOV1: LAI and FAPAR essential climate variables and FCOVER global time series capitalizing over existing products. Part1: Principles of development and production. Remote Sens. Environ. 137, 299–309.

Basuki, T.M., Skidmore, A.K., van Laake, P.E., van Duren, I., Hussin, Y. A., 2012. The potential of spectral mixture analysis to improve the estimation accuracy of tropical forest biomass. Geocarto Int. 27, 329–345.

Bruijnzeel, L.A., Proctor, J., 1995. Hydrology and biogeochemistry of tropical montane cloud forests: what do we really know?, in: Hamilton, L.S., Juvik, J.O., Scatena, F.N. (Eds.), Tropical Montane Cloud Forests. Springer, US, pp. 38–78.

Carlson, K.M., Curran, L.M., Asner, G.P., Pittman, A.M., Trigg, S.N., Marion Adeney, J., 2012. Carbon emissions from forest conversion by Kalimantan oil palm plantations. Nat. Clim. Chang. 3, 283–287.

Chen, J.M., Black, T.A., Adams, R.S., 1991. Evaluation of hemispherical photography for determining plant area index and geometry of a forest stand. Agric. For. Meteorol. 56, 129–143.

867 Chen, J.M., Cihlar, J., 1995. Plant canopy gap-size analysis theory for improving optical
868 measurements of leaf-area index. Appl. Opt. 34, 6211.

869 Claverie, M., Vermote, E.F., Franch, B., Masek, J.G., 2015. Evaluation of the Landsat-5 TM and
870 Landsat-7 ETM + surface reflectance products. Remote Sens. Environ. 169, 390–403.

871 Coomes, D.A., Dalponte, M., Jucker, T., Asner, G.P., Banin, L.F., Burslem, D.F.R.P., Lewis, S.L.,
872 Nilus, R., Phillips, O., Phuag, M.-H., Qiee, L., 2017. Area-based vs tree-centric approaches
873 to mapping forest carbon in Southeast Asian forests with airborne laser scanning data.
874 Remote Sens. Environ. 194, 77–88.

875 DeVries, B., Decuyper, M., Verbesselt, J., Zeileis, A., Herold, M., Joseph, S., 2015. Tracking
876 disturbance-regrowth dynamics in tropical forests using structural change detection and
877 Landsat time series. Remote Sens. Environ. 169, 320–334.

878 Ewers, R.M., Didham, R.K., Fahrig, L., Ferraz, G., Hector, A., Holt, R.D., Kapos, V., Reynolds,
879 G., Sinun, W., Snaddon, J.L., Turner, E.C., 2011. A large-scale forest fragmentation
880 experiment: the Stability of Altered Forest Ecosystems Project. Philos. Trans. R. Soc. B Biol.
881 Sci. 366, 3292–3302.

882 Feret, J.B., Asner, G.P., 2011a. Spectroscopic classification of tropical forest species using
883 radiative transfer modeling. Remote Sens. Environ. 115, 2415–2422.

884 Feret, J.B., François, C., Gitelson, A., Asner, G.P., Barry, K.M., Panigada, C., Richardson, A.D.,
885 Jacquemoud, S., 2011b. Optimizing spectral indices and chemometric analysis of leaf
886 chemical properties using radiative transfer modeling. Remote Sens. Environ. 115, 2742–
887 2750.

888 Feret, J.B., François, C., Asner, G.P., Gitelson, A.A., Martin, R.E., Bidel, L.P.R., Ustin, S.L., le
889 Maire, G., Jacquemoud, S., 2008. PROSPECT-4 and 5: Advances in the leaf optical
890 properties model separating photosynthetic pigments. Remote Sens. Environ. 112, 3030–
891 3043.

892 Foody, G.M., Boyd, D.S., Cutler, M.E.J., 2003. Predictive relations of tropical forest biomass from
893 Landsat TM data and their transferability between regions. Remote Sens. Environ. 85, 463–
894 474.

895 Fuller, D.O., 2006. Tropical forest monitoring and remote sensing: A new era of transparency in
896 forest governance? Singap. J. Trop. Geogr. 27, 15–29.

897 Ganguly, S., Nemani, R.R., Zhang, G., Hashimoto, H., Milesi, C., Michaelis, A., Wang, W.,
898 Votava, P., Samanta, A., Melton, F., Dungan, J.L., Vermote, E., Gao, F., Knyazikhin, Y.,
899 Myneni, R.B., 2012. Generating global Leaf Area Index from Landsat: Algorithm
900 formulation and demonstration. Remote Sens. Environ. 122, 185–202.

901 Gao, B.C., 1996. NDWI—A normalized difference water index for re-mote sensing of vegetation
902 liquid water from space. Remote Sens. Environ. 58, 257–266.

903 Gastellu-Etchegorry, J., 1996. Modeling radiative transfer in heterogeneous 3-D vegetation
904 canopies. Remote Sens. Environ. 58, 131–156.

905 Gaveau, D.L.A., Sheil, D., Husnayaen, Salim, M.A., Arjasakusuma, S., Ancrenaz, M., Pacheco,
906 P., Meijaard, E., 2016. Rapid conversions and avoided deforestation: examining four
907 decades of industrial plantation expansion in Borneo. Sci. Rep. 6, 32017.

908 Geng, J., Chen, J.M., Tu, L.L., Tian, Q.J., Wang, L., Yang, R.R., Yang, Y.J., Huang, Y., Fan,
909 W.L., Lv, C.G., Zheng, G., 2016. Influence of the exclusion distance among trees on gap
910 fraction and foliage clumping index of forest plantations. Trees - Struct. Funct. 30, 1683–
911 1693.

912 Gonsamo, A., Walter, J.M.N., Pellikka, P., 2011. CIMES: A package of programs for determining
913 canopy geometry and solar radiation regimes through hemispherical photographs. Comput.
914 Electron. Agric. 79, 207–215.

915 Hansen, M.C., Potapov, P. V, Moore, R., Hancher, M., Turubanova, S.A., Tyukavina, A., Thau,
916 D., Stehman, S. V, Goetz, S.J., Loveland, T.R., Kommareddy, A., Egorov, A., Chini, L.,
917 Justice, C.O., Townshend, J.R.G., 2013. High-Resolution Global Maps of 21st-Century
918 Forest Cover Change. Science. 342, 850–853. Data available on-line
919 from:http://earthenginepartners.appspot.com/science-2013-global-forest.

920 Hardwick, S.R., Toumi, R., Pfeifer, M., Turner, E.C., Nilus, R., Ewers, R.M., 2015. The
921 relationship between leaf area index and microclimate in tropical forest and oil palm
922 plantation: Forest disturbance drives changes in microclimate. Agric. For. Meteorol. 201,
923 187–195.

924 Hijmans, R.J., 2016. raster: Geographic Data Analysis and Modeling. R package version 2.5-8.
925 https://CRAN.R-project.org/package=raster

926 Houghton, R.A., Byers, B., Nassikas, A.A., 2015. A role for tropical forests in stabilizing
927 atmospheric CO2. Nat. Clim. Chang. 5, 1022–1023.

928 Huete, A., Didan, K., Miura, T., Rodriguez, E.P., Gao, X., Ferreira, L.G., 2002. Overview of the
929 radiometric and biophysical performance of the MODIS vegetation indices. Remote Sens.
930 Environ. 83, 195–213.

931 Iooss, B., Lemaître, P., 2015. A review on global sensitivity analysis methods, in: Uncertainty
932 Management in Simulation-Optimization of Complex Systems. Springer, US, pp. 101–122.

933 Jacquemoud, S., Baret, F., 1990. PROSPECT: A model of leaf optical properties spectra. Remote
934 Sens. Environ. 34, 75–91.

935 Jacquemoud, S., Ustin, S.L., Verdebout, J., Schmuck, G., Andreoli, G., Hosgood, B., 1996.
936 Estimating leaf biochemistry using the PROSPECT leaf optical properties model. Remote
937 Sens. Environ. 56, 194–202.

938 Jacquemoud, S., Verhoef, W., Baret, F., Bacour, C., Zarco-Tejada, P.J., Asner, G.P., François, C.,
939 Ustin, S.L., 2009. PROSPECT+SAIL models: A review of use for vegetation
940 characterization. Remote Sens. Environ. 113, S56–S66.

941 Jansen, M.J.W., 1999. Analysis of variance designs for model output. Comput. Phys. Commun.
942 117, 35–43.

Jonckheere, I., Nackaerts, K., Muys, B., Coppin, P., 2005. Assessment of automatic gap fraction estimation of forests from digital hemispherical photography. Agric. For. Meteorol. 132, 96–114.

Key, C.H., Benson, N.C., 2006. Landscape Assessment (LA). FIREMON: Fire effects monitoring and inventory system. Gen. Tech. Rep. RMRS-GTR-164-CD. Fort Collins, CO.

Knyazikhin, Y., Schull, M.A., Stenberg, P., Mõttus, M., Rautiainen, M., Yang, Y., Marshak, A., Latorre Carmona, P., Kaufmann, R.K., Lewis, P., Disney, M.I., Vanderbilt, V., Davis, A.B., Baret, F., Jacquemoud, S., Lyapustin, A., Myneni, R.B., 2013. Hyperspectral remote sensing of foliar nitrogen content. Proc. Natl. Acad. Sci. U. S. A. 110, E185-92.

Koh, L.P., Miettinen, J., Liew, S.C., Ghazoul, J., 2011. Remotely sensed evidence of tropical peatland conversion to oil palm. Proc. Natl. Acad. Sci. U. S. A. 108, 5127–32.

Korhonen, L., Heikkinen, J., 2009. Automated analysis of in situ canopy images for the estimation of forest canopy cover. For. Sci. 55, 323–334.

Korhonen, L., Korpela, I., Heiskanen, J., Maltamo, M., 2011. Airborne discrete-return LIDAR data in the estimation of vertical canopy cover, angular canopy closure and leaf area index. Remote Sens. Environ. 115, 1065–1080.

Kuusinen, N., Lukeš, P., Stenberg, P., Levula, J., Nikinmaa, E., Berninger, F., 2014. Measured and modelled albedos in Finnish boreal forest stands of different species, structure and understory. Ecol. Modell. 284, 10–18.

Kuusk, A., Nilson, T., 2000. A directional multispectral forest reflectance model. Remote Sens. Environ. 72, 244–252.

Langner, A., Samejima, H., Ong, R.C., Titin, J., Kitayama, K., 2012. Integration of carbon conservation into sustainable forest management using high resolution satellite imagery: A case study in Sabah, Malaysian Borneo. Int. J. Appl. Earth Obs. Geoinf. 18, 305–312.

Lang, A.R.G., Xiang, Y., 1986. Estimation of leaf area index from transmission of direct sunlight in discontinuous canopies. Agric. For. Meteorol. 37, 229–243.

Latorre-Carmona, P., Knyazikhin, Y., Alonso, L., Moreno, J.F., Pla, F., Yan, Y., 2014. On hyperspectral remote sensing of leaf biophysical constituents: Decoupling vegetation structure and leaf optics using CHRIS-PROBA data over crops in barrax. IEEE Geosci. Remote Sens. Lett. 11, 1579–1583.

Lehnert, L.W., Meyer, H., Bendix, J., 2016. hsdar: Manage, analyse and simulate hyperspectral data in R. R package version 0.5.0.

MacDicken, K.G., 2015. Global Forest Resources Assessment 2015: What, why and how? For. Ecol. Manage. 352, 3–8.

Margono, B.A., Potapov, P. V, Turubanova, S., Stolle, F., Hansen, M.C., 2014. Primary forest cover loss in Indonesia over 2000–2012. Nat. Clim. Chang. 4, 1–6.

Masek, J.G., Vermote, E.F., Saleous, N.E., Wolfe, R., Hall, F.G., Huemmrich, K.F., Gao, F., Kutler, J., Lim, T.K., 2006. A landsat surface reflectance dataset for North America, 1990-2000. IEEE Geosci. Remote Sens. Lett. 3, 68–72.

McMorrow, J., 2001. Linear regression modelling for the estimation of oil palm age from Landsat TM. Int. J. Remote Sens. 22, 2243–2264.

McMorrow, J.M., 1995. Relation of oil palm spectral response to stand age. Int. J. Remote Sens. 16, 3203–3209.

Morel, A.C., Fisher, J.B., Malhi, Y., 2012. Evaluating the potential to monitor aboveground biomass in forest and oil palm in Sabah, Malaysia, for 2000-2008 with Landsat ETM plus and ALOS-PALSAR. Int. J. Remote Sens. 33, 3614–3639.

Mõttus, M., Stenberg, P., 2008. A simple parameterization of canopy reflectance using photon recollision probability. Remote Sens. Environ. 112, 1545–1551.

Myneni, R.., Hoffman, S., Knyazikhin, Y., Privette, J.., Glassy, J., Tian, Y., Wang, Y., Song, X., Zhang, Y., Smith, G.., Lotsch, A., Friedl, M., Morisette, J.., Votava, P., Nemani, R.., Running, S.., 2002. Global products of vegetation leaf area and fraction absorbed PAR from year one of MODIS data. Remote Sens. Environ. 83, 214–231.

Nilson, T., 1999. Inversion of gap frequency data in forest stands. Agric. For. Meteorol 98/99, 437–448.

Olivas, P.C., Oberbauer, S.F., Clark, D.B., Clark, D.A., Ryan, M.G., O'Brien, J.J., Ordoñez, H., 2013. Comparison of direct and indirect methods for assessing leaf area index across a tropical rain forest landscape. Agric. For. Meteorol. 177, 110–116.

Pfeifer, M., Gonsamo, A., Disney, M., Pellikka, P., Marchant, R., 2012. Leaf area index for biomes of the Eastern Arc Mountains: Landsat and SPOT observations along precipitation and altitude gradients. Remote Sens. Environ. 118, 103–115.

Pfeifer, M., Kor, L., Nilus, R., Turner, E., Cusack, J., Lysenko, I., Khoo, M., Chey, V., Chung, A.Y.C., Ewers, R.M., 2016. Mapping the structure of Borneo's tropical forests across a degradation gradient. Remote Sens. Environ. 176, 84–97.

Pfeifer, M., Lefebvre, V., Gonsamo, A., Pellikka, P.K.E., Marchant, R., Denu, D., Platts, P.J., 2014. Validating and linking the GIMMS leaf area index (LAI3g) with environmental controls in tropical Africa. Remote Sens. 6, 1973–1990.

Popkin, G., 2016. Satellite alerts track deforestation in real time. Nat. news 392–393.

Propastin, P., 2013. GIScience & Remote Sensing Large-scale mapping of aboveground biomass of tropical rainforest in Sulawesi, Indonesia using Landsat ETM+ and MODIS data. GIScience Remote Sens. 50, 633–651.

Propastin, P., Erasmi, S., 2010. A physically based approach to model LAI from MODIS 250m data in a tropical region. Int. J. Appl. Earth Obs. Geoinf. 12, 47–59.

Pujol, G., Iooss, B., Janon A., Boumhaout, K., Da Veiga, S., Delage, T., Fruth, J., Gilquin, L., Guillaume, J., Le Gratiet, L., Lemaitre, P., Nelson, B.L., Monari, F., Oomen, R., Ramos, B.,

Roustant, O., Song, E., Staum, J., Touati, T., Weber, F., 2017. sensitivity: Global Sensitivity Analysis of Model Outputs. R package version 1.14.0. https://CRAN.R-project.org/package=sensitivity

R Core Team, 2016. R: A language and environment for statistical computing.

Rautiainen, M., Stenberg, P., 2015. On the angular dependency of canopy gap fractions in pine, spruce and birch stands. Agric. For. Meteorol. 206, 1–3.

Rautiainen, M., Stenberg, P., 2005. Application of photon recollision probability in coniferous canopy reflectance simulations. Remote Sens. Environ. 96, 98–107.

Rautiainen, M., Stenberg, P., Nilson, T., 2005. Estimating canopy cover in scots pine stands. Silva Fenn. 39, 137–142.

Ridler, T.W., Calvard, S., 1978. Picture thresholding using an iterative selection method. IEEE Trans. Syst. Man. Cybern. 630–632.

Ritchie, R.J., Runcie, J.W., 2014. A portable reflectance-absorptance-transmittance meter for photosynthetic work on vascular plant leaves. Photosynthetica 52, 614–626.

Ross, J., 1981. The radiation regime and architecture of plant stands. Dr. W. Junk Publishers, The Hague.

Rudel, T.K., Defries, R., Asner, G.P., Laurance, W.F., 2009. Changing drivers of deforestation and new opportunities for conservation. Conserv. Biol. 23, 1396–1405.

Ryu, Y., Nilson, T., Kobayashi, H., Sonnentag, O., Law, B.E., Baldocchi, D.D., 2010. On the correct estimation of effective leaf area index : Does it reveal information on clumping effects ? Agric. For. Meteorol. 150, 463–472.

Saltelli, A., Annoni, P., Azzini, I., Campolongo, F., Ratto, M., Tarantola, S., 2010. Variance based sensitivity analysis of model output. Design and estimator for the total sensitivity index. Comput. Phys. Commun. 181, 259–270.

Samanta, A., Knyazikhin, Y., Xu, L., Dickinson, R.E., Fu, R., Costa, M.H., Saatchi, S.S., Nemani, R.R., Myneni, R.B., 2012. Seasonal changes in leaf area of Amazon forests from leaf flushing and abscission. J. Geophys. Res. Biogeosciences 117, 1–13.

Schull, M.A., Knyazikhin, Y., Xu, L., Samanta, A., Carmona, P.L., Lepine, L., Jenkins, J.P., Ganguly, S., Myneni, R.B., 2011. Canopy spectral invariants, Part 2: Application to classification of forest types from hyperspectral data. J. Quant. Spectrosc. Radiat. Transf. 112, 736–750.

Serbin, S.P., 2013. Rprospect: R functions for running PROSPECT family of leaf radiative transfer models. R package version 0.87.

Slik, J.W.F., Aiba, S.I., Brearley, F.Q., Cannon, C.H., Forshed, O., Kitayama, K., Nagamasu, H., Nilus, R., Payne, J., Paoli, G., Poulsen, A.D., Raes, N., Sheil, D., Sidiyasa, K., Suzuki, E., van Valkenburg, J.L.C.H., 2010. Environmental correlates of tree biomass, basal area, wood specific gravity and stem density gradients in Borneo's tropical forests. Glob. Ecol. Biogeogr. 19, 50–60.

Smolander, S., Stenberg, P., 2005. Simple parameterizations of the radiation budget of uniform broadleaved and coniferous canopies. Remote Sens. Environ. 94, 355–363.

Sobol, I.M., 1993. Sensitivity estimates for nonlinear mathematical models. Math. Model. Comput. Exp. 1, 407–414.

Stenberg, P., Lukeš, P., Rautiainen, M., Manninen, T., 2013. A forest albedo model based on spectral invariants. Remote Sens. Environ. 137, 12-16.

Stenberg, P., Mõttus, M., Rautiainen, M., 2016. Photon recollision probability in modelling the radiation regime of canopies - A review. Remote Sens. Environ. 183, 98–108.

Sullivan, M.J.., Talbot, J., Lewis, S.L., Phillips, O.L., Qie, L., Begne, S.K., Chave, J., Cuni Sanchez, A., Hubau, W., Lopez-Gonzalez, G., Miles, L., Monteagudo-Mendoza, A., Sonké, B., Sunderland, T., ter Steege, H., White, L.J.T., Affum-Baffoe, K., Aiba, S.I., Almeida, E., de Oliveira, E.A., Alvarez-Loayza, P., Dàvilla, E.A., Andrade, A., Aragão, L.E.O.C., Ashton, P., Aymard C., G.A., Baker, T.R., Balinga, M., Banin, L., Baraloto, C., Bastin, J.-F., Berry, N.J., Bogaert, J., Bonal, D., Bongers, F., Brienen, R.J.W., Camargo, J.L.C., Cerôn, C., Moscoso, V.C., Chezeaux, E., Clark, C.J., Pacheco, A.C., Comiskey, J.A., Cornejo Valverde, F., Honorio Coronado, E.N., Dargie, G., Davies, S.J., De Cannière, C., Djuikouo, M.N.K., Doucet, J.-L., Erwin, T., Silva-Espejo, J., Ewango, C.E.N., Fauset, S., Feldpausch, T.R., Herrera, R., Gilpin, M., Gloor, E., Hall, J., Harris, D.J., Hart, T.B., Kartawinata, K., Kho, L.K., Kitayama, K., Laurance, S.G., Laurance, W.F., Leal, M.E., Lovejoy, T., Lovett, J.C., Lukasu, F.M., Makana, J.-R., Malhi, Y., Maracahipes, L., Marimon, B.S., Marimon-Junior, B.H., Marshall, A.R., Morandi, P.S., Mukendi, J.T., Mukinzi, J., Nilus, R., Núñez Vargas, P., Pallqui Camacho, N.C., Pardo, G., Pena-Claros, M., Pétronelli, P., Pickavance, G., Poulsen, A.D., Poulsen, J.R., Primack, R.B., Priyadi, H., Quesada, C.A., Reitsma, J.M., Salim, K.A., Salomão, R.P., Samsoedin, I., Sheil, D., Sierra, R., Silveira, M., Slik, J.W.F., Steel, L., Taedoumg, H.E., Tan, S., Terborgh, J., Thomas, S.C., Toledo, M., Umunay, P., Gamarra, L.V., Guimarães Vieira, I.C., Vos, V., Wang, O., Willcock, S., Zemagho, L., 2017. Diversity and carbon storage accross the tropical forest biome. Sci. Rep. 7, 1–12.

Trichon, V., Walter, J.-M.N., Laumonier, Y., 1998. Identifying spatial patterns in the tropical rain forest structure using hemispherical photographs. Plant Ecol. 137, 227–244.

Tucker, C.J., 1979. Red and photographic infrared linear combinations for monitoring vegetation. Remote Sens. Environ. 8, 127–150.

United Nations Framework Convention on Climate Change, 2015. Adoption of the Paris Agreement. Paris. https://unfccc.int/resource/docs/2015/cop21/eng/l09r01.pdf

Van der Werf, G.R., Morton, D.C., DeFries, R.S., Oliver, J.G., Kasibhatla, P.S., Jackson, R.B., Collatz, G.J., Randerson, J.T., 2009. CO2 emissions from forest loss. Nat. Geosci. 2, 737–738.

Van Reuler, H., 1987. Soil studies in the Bukit Raya nature reserve, in: Nooteboom, H.P. (Ed.), Report of the 1982-1983 Bukit Raya Expedition. Rijksherbarium, Leiden, the Netherlands, pp. 7–23.

Verhoef, W., Bach, H., 2007. Coupled soil-leaf-canopy and atmosphere radiative transfer modeling to simulate hyperspectral multi-angular surface reflectance and TOA radiance data. Remote Sens. Environ. 109, 166–182.

Verstraete, M.M., Pinty, B., Myneni, R.B., 1996. Potential and Limitations of Information Extraction on the Terrestrial Biosphere from Satellite Remote Sensing. Remote Sens. Environ. 58, 201–214.

Welles, J.M., Cohen, S., 1996. Canopy structure measurement by gap fraction analysis using commercial instrumentation. J. Exp. Bot. 47, 1335–1342.

Welles, J.M., Norman, J.M., 1991. Instrument for Indirect Measurement of Canopy Architecture. Agron. J. 83, 818–825.

Wheeler, D., Hammer, D., Kraft, R., Steele, A., 2014. Satellite-Based Forest Clearing Detection in the Brazilian Amazon: FORMA, DETER, and PRODES. Washington, DC.

Wijedasa, L.S., Sloan, S., Michelakis, D.G., Clements, G.R., 2012. Overcoming limitations with landsat imagery for mapping of peat swamp forests in sundaland. Remote Sens. 4, 2595–2618.

World Agroforestry Center (ICRAF). A Globally Distributed Soil Spectral Library Visible Near Infrared Diffuse Reflectance Spectra. http://www.isric.org/data/icrafisric-spectral-library

Yáñez-rausell, L., Rautiainen, M., Clevers, J.G.P.W., Lukeš, P., Hanuš, J., Schaepman, M.E., Member, S., 2015. Estimation of Spruce Needle-Leaf Chlorophyll Content Based on DART and PARAS Canopy Reflectance Models. IEEE J. Sel. Top. Appl. Earth Obs. Remote Sens. 8, 1534–1544.

Zhang, Y., Chen, J.M., Miller, J.R., 2005. Determining digital hemispherical photograph exposure for leaf area index estimation. Agric. For. Meteorol. 133, 166–181.